Summer 8-16-2024

Comparison of the Hygrothermal Properties of Mechanically Fastened and Adhesive Bonded Wood-Fiber Insulated Panels

Jake Snow
Universtiy of Maine, jake.snow@maine.edu

COMPARISON OF THE HYGROTHERMAL PROPERTIES OF MECHANICALLY

FASTENED AND ADHESIVE BONDED WOOD-FIBER INSULATED PANELS

By

Jacob Snow

B.S. University of Maine, 2021

A THESIS

Submitted in Partial Fulfillment of the

Requirements for the Degree of

Master of Science

(in Forest Resources)

The Graduate School

The University of Maine

August 2024

Advisory Committee:

Ling Li, Assistant Professor of Sustainable Bioenergy Systems, Advisor

Benjamin Herzog, Senior Wood Technologist

Samuel Glass, Senior Forest Products Researcher

Stephen Shaler, Professor Emeritus of Sustainable Materials and Technology

Douglas Gardner, Professor of Sustainable Materials and Technology

UNIVERSITY OF MAINE GRADUATE SCHOOL LAND ACKNOWLEDGMENT

The University of Maine recognizes that it is located on Marsh Island in the homeland of Penobscot people, where issues of water and territorial rights, and encroachment upon sacred sites, are ongoing. Penobscot homeland is connected to the other Wabanaki Tribal Nations— the Passamaquoddy, Maliseet, and Micmac—through kinship, alliances, and diplomacy. The University also recognizes that the Penobscot Nation and the other Wabanaki Tribal Nations are distinct, sovereign, legal and political entities with their own powers of self-governance and self -determination.

COMPARISON OF THE HYGROTHERMAL PROPERTIES OF MECHANICALLY FASTENED AND ADHESIVE BONDED WOOD-FIBER INSULATED PANELS

By Jacob Snow

Thesis Advisor: Dr. Ling Li

An Abstract of the Thesis Presented
In Partial Fulfillment of the Requirements for the
Master of Science
(in Forest Resources)
August 2024

This study aimed to characterize the hygrothermal and material, i.e., physical and mechanical, properties of wood fiber insulation (WFI) that can be an alternative to fossil-based building insulation, targeting structural insulated panels, retrofit insulated panels, and a novel all wood structural insulated panel. The hygrothermal properties of rigid WFI boards with varying densities, 110, 140, and 180 kg/m^3, and one 140 kg/m^3 without paraffin wax treatment were evaluated following relevant ASTM standards. The hygrothermal properties measured were, porosity, water vapor transmission, liquid water absorption, and thermal conductivity at varying temperatures. Additionally, the tensile and block shear strength of WFI bonded to lumber, OSB, and WFI was evaluated using three different structural adhesives to select one adhesive for further prototyping. The porosity of the WFI varied from 85-92% and is primarily impacted by density and not the presence of wax in the composite. The permeability of the WFI ranged from 65 ng·s^{-1}m^{-1}Pa^{-1} to 90 ng·s^{-1}m^{-1}Pa^{-1} depending on the samples 'density. Liquid water absorption on a % volume basis ranged from 2.5 – 20%, both wax and density were impactful to the results. Thermal conductivity

coefficient (λ), ranged from 0.038 - 0.055 W/(m·K) depending on moisture content, average temperature, and density. 140 kg/m^3 WFI with wax was selected as a representative material for the mechanical property testing of WFI laminated to other substrates. The tensile-perpendicular to grain bond strength was 10-16 kPa with substrate being more impactful than adhesive type. The shear strength was 60-90 kPa again with substrate being more impactful than adhesive type. For all tests, the primary failure occurred within the insulation substrate illustrating the strength of the composite was not controlled by the adhesive layer, but instead the insulation lamina itself. The results of this body of work establish that all wood structural insulated panels have the potential to succeed when used properly as a component of novel bio-based buildings based on their competitive hygrothermal properties and no immediate issue presented in using construction adhesives to manufacture the panels. However, the work also shows that bio-based materials are variable and complex in their composition and interaction with the environment. Rigorous testing will be required to fully predict how WFI will perform in-situ in various climates and in more complex assemblies.

The built environment is one of the leading contributors to global CO_2 emissions and this margin is projected to grow. The materials that are used to construct a building are a major component of the associated carbon of a building. They represent the majority of embodied carbon and contribute to the rate at which operational carbon is generated. High performance, renewable, and carbon sequestering materials will be critical as the world continues to develop and demand more housing. This study reports the continuation of the development of a wood fiber-insulated panel (WIP) that offers a high-performance envelope without requiring hydro-carbon materials, by utilizing an all-wood design constructed with adhesives as opposed to mechanical fasteners. This design

eliminates the cost and thermal reduction associated with the fasteners while retaining thermal performance. To this end, a WIP prototype was developed and manufactured along with two control wall assemblies: a similar wall assembly to the WIP with fasteners instead of adhesive (to laminate the WIP components), and an assembly made with polystyrene insulation. These assemblies were then evaluated in a simulated winter environment in climate zone 6A for hygrothermal performance. Temperature, relative humidity, and moisture content data were collected throughout the panels, and heat flux measurements were used to evaluate the impact of the fastener penetrations on thermal bridging. The WIP panels were found to perform as well or better than the control panels when evaluated for moisture interactions and insulative performance. Primarily, the use of structural adhesives within the assembly did not create a location where moisture accumulated. The mechanically fastened wood insulated panels performed well and managed bulk moisture very effectively. The polystyrene insulated panels performed well thermally but had high moisture levels between layers of insulation. Through these results it can be seen that a prefabricated all-wood panel could be successfully implemented as a high performance and environmentally friendly solution to growing housing demands and the requirements for more efficient buildings. Further analysis of the life cycle of these panels and complex hygrothermal simulations to investigate other potential designs and climate zones will be necessary to further develop this product.

DEDICATION

This thesis is dedicated to my partner, who has endured this process with me. Despite all the stress and absences, I put you through these last few years you stayed by me, and I couldn't have done it without you. Thank you for being my first editor, my biggest fan, and a constant source of inspiration. This thesis is also dedicated to my cat, who was more disruptive than anything else, but still a critical part of this undertaking.

ACKNOWLEDGEMENTS

TABLE OF CONTENTS

LIST OF FIGURES

LIST OF TABLES

LIST OF EQUATIONS

CHAPTER 1

CHARACTERIZATION OF WOOD FIBER INSULATION FOR THE DEVELOPMENT OF WOOD-FIBER INSULATED PANELS (WIPS) FOR USE IN BUILDING ENVELOPES: COMPONENT MECHANICAL AND PHYSICAL TESTING

1. INTRODUCTION

The built environment is responsible for 40% of global CO_2 emissions per year, an equivalent of 14.6 gigatons of CO_2 per year. 9.9 gigatons of that 14.6 are directly related to building operations (Architecture 2030, 2021). In addition to the emissions related to buildings, the industry consumes massive amounts of natural resources and many of the materials used and produced in construction are detrimental to human health (Fernando Pacheco Torgal et al., 2012). One of the primary methods of addressing this problem is through modification of the building envelope. Improving the thermal envelope of a building can drastically reduce its operating carbon footprint. Prefabricated insulation panels with insulation and sheathing combined into a single panel are a popular and effective product at addressing thermal loss by retrofitting existing buildings and building new envelopes. However, addressing this issue with fossil fuel-based insulation materials can be counterproductive to solving this problem by increasing the embodied carbon footprint of the building. Polystyrene foam-based insulation materials, a common core for structural insulated panels (SIPs), can have an embodied carbon of 4.2-5.8 kg CO_2 per kg of material (Kunic, 2017) and are formulated using non-renewable hydrocarbon oils. As the built environment grows, the materials we choose to use will become more and more important as we need to be more decisive regarding environmental impacts. Utilizing, developing, and researching bio-based alternatives to petroleum-based products are some of the most impactful steps we can take at the moment to reduce our impact on the local, and global environment.

1

Wood fiber insulation (WFI) is an insulation product manufactured from wood fibrillated in either a wet or dry process (Veitmans et al. 2016). The fibers can be used in a loose form for blown-in insulation or formed into boards for a between stud or external-continuous-envelope and prefabricated applications. WFI is an environmentally friendly alternative material to carbon emitting materials; carbon sequestered by a growing tree is retained when the tree is processed into building materials as the carbon sequestered by the trees as they are growing is stored in the material for the life of the building (Lawrence et al. 2013). This negative carbon input is a critical factor when evaluating the equivalent CO_2 emissions associated with a building, given the massive volume that could potentially be sequestered in a multi-family development over the lifetime of the building. The fibers can be made using a breadth of species and using timber processing residuals. This flexibility further improves the environmental impact of these materials by rerouting waste streams from landfills and furnaces and also improves timber basket markets by reducing difficult waste streams (O'Dwyer et al. 2018). WFI is non-toxic while handling and cutting the final product, in comparison to the irritating and toxic materials generated by traditional insulation materials (Pacheco-Torgal et al. 2012). WFI has already gained market acceptance in some parts of Europe, where it was originally developed. WFI performs similarly to other foams, such as expanded polystyrene (EPS) and extruded polystyrene (XPS), for certain properties, e.g., thermal resistance while offering advantages in other aspects, such as water vapor permeance. While WFI offers many advantages in terms of carbon emissions and moisture performance, there are some disadvantages to using the material. The first and foremost is that it is less insulative than other non-renewable options like mineral wool. The same level of insulation can be achieved using WFI, but it requires a thicker layer. A second prominent disadvantage to WFI is its density. In order

for the boards to be handleabe they need to be manufactured at densities several times that of foam boards. This combination of increased thickness and increased weight can make the assemblies cumbersome and difficult to handle. However, this problem can be mitigated by manufacturing the envelope offsite and then craning the sections into place if the assemblies require it. Panelization in this manner offers many other benefits for the building's performance and carbon budget as well.

Structural insulated panels (SIPs) are a common solution for high performance buildings. These panels are prefabricated assemblies of two or three layers, a skin on one or both sides (typically faced OSB) with a core of XPS insulation. These layers are then affixed to each other with structural adhesives. If WFI board is used as a drop-in insulation panel to replace XPS/EPS in SIPs, retrofit insulated panels (RIPs), and novel wood fiber insulated panels (WIPs) (products currently being developed by the authors), the bonding performance of WFI and wood-based skin materials, such as oriented strand board (OSB) and cross-laminated timber (CLT) panels, plays a vital role in maintaining the integrity of the panel products. There are a number of adhesives that can potentially be used to manufacture SIPs and RIPs; Phenol -formaldehyde, polyurethane, polyether and isocyanate-based adhesives are just a few examples. These adhesives must be qualified for use under International Building Codes, specifically ICC-ES AC05 (ICC Evaluation Service, 2020). There is a lack of adequate information addressing the bonding performance between wood fiber insulation and wood-based products. The open porous nature of the WFI may impact the bond strength as compared to standard bonding of wood to wood or wood to polyurethane foams, attributable to the increased absorbance of the adhesive prior to curing. This information could be critical to the successful development of all wood structural insulated panels

and other novel adhesively bonded WFI assemblies.

The assessment of how building materials react when exposed to temperature and moisture gradients (generally referred to as "hygrothermal behavior") is critical to the successful estimation of building durability, operational energy efficiency, and occupant comfort (Cetiner, 2018). If such hygrothermal properties of the materials are not assessed in a holistic way and the appropriate solutions integrated into building design, then the resulting building may suffer from excess energy use as a result of heat loss through the envelope, and inefficient indoor climate conditioning. The building may also experience structural damage from condensation within the insulation layer and elevated moisture content, e.g. leading to decay or mold which will lead to poor indoor air quality and an unhealthy environment (A.Brambilla, 2020). High performance buildings that are tight and have thick impermeable insulation layers are at particular risk, as any moisture introduced cannot escape the envelope. This behavior considers the simultaneous and interdependent absorption, storage, and release, of both heat and moisture (Cetiner, 2018). A porous hygroscopic building material, such as WFI in this study, after some period exposed to a given temperature and relative humidity, will reach a state of equilibrium with this environment, exchanging the water vapor in its pores with the ambient air. This equilibrium is also impacted by the current state of the material, in that if it is drying then it will reach a different equilibrium than when it is wetting. This phenomenon is a result of the interaction of liquid and vaporous water within the pores bonding with the material (Belakroum et al., 2017; Hameury, 2005; Meissner et al., 2010; Osanyintola et al., 2006; Salonvaara et al., 2004; Simonson et al., 2004a; Simonson et al., 2004b). These bonds also impact the movement of energy through the material as the bonds take energy to form and release energy as they break (Koizumi et al., 2017; Faghri & Zhang, 2006). At the assembly level and whole building level, the hygrothermal performance and energy consumption of building

envelopes with different configurations and in various climate zones are usually simulated by solving combined heat and moisture transfer equations using WUFI and EnergyPlus software (Ciancio et al., 2018; Karagiozis et al., 2001). Specifically, the input material properties have a large influence on the reliability and accuracy of the modeling results.

This study aimed to conduct material characterizations of WFI materials that can be an alternative to fossil-based building insulation materials, targeting SIPs, RIPs, and WIPs. If successful this will provide data for the industry to support the adoption of novel or new to the region products, easing their entry in the space. First, the hygrothermal and physical properties of WFI rigid boards with three densities (110, 140, and 180 kg/m^3) and one (140 kg/m^3) without paraffin wax treatment were evaluated following relevant ASTM standards. These properties were porosity, water vapor permeability, liquid water retention, and thermal conductivity. Each of these properties influence how the insulation acts in a building and their use conditions. Porosity, being the volume of a material that consists of open spaces, directly influences moisture, air, and thermal relations. Water vapor permeability, the speed at which water vapor passes through a given thickness of material, plays a critical role in the design of a building envelope and is listed with most building envelope products. Liquid water retention, the weight and volume of water retained by the material, can be used to prescribe use conditions and hazards when handling the material. Lastly, the thermal conductivity, the amount of energy required to raise the temperature of a given area of material, is the single most heavily weighted factor when designing a building envelope.

In addition to characterizing the hygrothermal behavior of WFI, the bonding performance of a representative WFI product (140 kg/m^3, with paraffin wax treatment) with two face materials, lumber and OSB, bonded with three structural adhesives (a two-part emulsion polymer isocyanate

and two types of one-component polyurethane) was assessed to select one adhesive based on the tensile bond strength and shear strength results. These two mechanical properties are of particular importance for wall assemblies given the orientation and will act as screener tests for the composite prior to further mechanical testing of creep mechanics and comparative studies to existing panel composites. The results of WFI samples were documented for the WIPs design, manufacturing, and hygrothermal and energy modeling analysis.

2. MATERIALS AND METHODS

2.1. **Materials**

2.1.1. **Wood Fiber Insulation**

The WFI materials used in this study were sourced from a European manufacturer and made using a dry process. The boards are formulated from softwood fibers and pressed into boards after a mix of adhesive and other additives, often water repellants or fire retarders, are sprayed onto the dry fibers. The WFI boards are manufactured with polymeric methylene diphenyl diisocyanate (pMDI), some of the boards have paraffin wax as an additive to reduce the water uptake (De Ligne et al., 2022; Kirsch et al., 2018). As shown in Table 2. 1, the panels had nominal densities of 110, 140, and 180 kg/m^3 with a variant of the 140 boards without paraffin wax. These densities were chosen as they represent the range of densities commonly used for continuous wall envelopes by the building industry. The thicknesses of the insulations are as follows, 3.81 cm for the 110 and 180 boards and 6.03 cm for the 140 boards. The moisture content of WFI panels as received was within the range of 7% to 9% (Table 2. 1.)

2.1.2. Oriented Strand Board (OSB)

OSB panels were sourced from a local retailer. The OSB was manufactured with Southern Yellow Pine wood strands, pMDI adhesive and wax to manage moisture. In Table 2. 1, the OSB used in this study had a nominal thickness of 1.11 cm. The moisture content of OSB was $9.8 \pm 0.2\%$ and the corresponding density of the OSB was 601 ± 20 kg/m^3 (mean±SD).

2.1.3. Lumber

Dimensional lumber, a commercial mix of spruce, pine and fir (SPF-S), was used in this study to simulate bonding to a cross-laminated timber panel. The lumber was conditioned to ≈12% moisture content prior to use. The density of lumber samples at $11.7 \pm 0.6\%$ MC was 337 ± 6 kg/m^3 (mean±SD).

Table 1. 1 List of materials used as substrates

Materials	Nominal Density (kg/m^3)	MC, %	Thickness (cm)	Wax	Code
WFI	110	7.5	3.81	Y	110W
	140	7.5	6.03	Y	140W
	140	8.45	6.03	N	140NW
	180	7.5	3.81	Y	180W
OSB	600	9.8	1.11	Y	OSB
Lumber	340	11.7	3.49	N	SPF

2.1.4. Adhesives

Three adhesives were , evaluated. The first was a two-part Emulsion Polymer Isocyanate (EPI) that is used in manufacturing various engineered wood products such as MDF and plywood. The EPI adhesive meets requirements for wet-use wood bonding applications under ASTM D5751: *Specification for Adhesives Used for Laminate Joints in Nonstructural Lumber Products* (ASTM International, 2019). The second adhesive was a rapid set single component polyurethane (PUR) adhesive commonly used for SIP manufacturing. Finally, a slow set single component polyurethane adhesive commonly used for engineered wood products manufacturing were also used as part of the evaluation. The rapid set PUR has ICC-ES AC05 code approval for structural insulated panels under Code Report ESR-1002. The slow set PUR fulfils the requirements of ASTM E119: *Standard Test Methods for Fire Tests of Building Construction and Materials* (ASTM International, 2022) and fulfills all requirements of AITC 405-2008 (Standard for Adhesives for Use in Structural Glued Laminated Timber) (APA, 2013). Table 2. 2 summarizes the application information of adhesives.

Table 1. 2: Adhesive Types, and Manufacturing Parameters

Adhesive	Code	Primer	Application Rate	Press time
Polyurethane	PUR-S	Yes	249 g/m^2	2 hours
Polyurethane	PUR-R	Water	215 g/m^2	8 minutes
Emulsion Polymer Isocyanate	EPI	No	245 g/m^2	16 hours

2.2.   Methods for Physical and Hygrothermal Properties of WFI

2.2.1. Porosity of WFI

The porosity of WFI samples is determined using the skeletal volume [defined as the sum of the volumes of the solid material and closed (or blind) pores within the material (if any)] and the envelope volume, i.e., the sum of the volumes of the solid material and all types of pores within the material, of a sample per Equation 1. 1. The nominal dimensions of WFI samples were 2.54 x 2.54 x 7.62 cm. The four WFI types were 110W, 140W, 140NW, and 180W. Before testing, all samples were oven-dried to prevent any moisture from influencing the test results. The skeletal volume of WFI was determined by a gas pycnometer (AccuPyc II 1340, Micromeritics), which measures the skeletal volume of a material by gas (helium) displacement using the volume-pressure relationship of Boyle's Law. The operation of the gas pycnometer followed the instruction provided by Micromeritics. This subtractive method provides the closest approximation of skeletal volume for a porous material (Donato & Lazzara, 2012). The apparent volume of WFI was measured using a digital caliper. The measurement of both skeletal volume and true volume was repeated three times for each sample with three replicates of each material type. Samples represented the entire vertical thickness of the panels and were cut from unique panels.

$$Porosity, \% = 100 * \left[1 - \left(\frac{V_a}{V_s} \right) \right]$$

Equation 1. 1

Where,

$V_a = Apparent\ volume, cm^3$

$V_s = Skeletal\ volume, cm^3$

2.2.2. Water Vapor Transmission Rate, Permeance, and Permeability of WFI

The water vapor transmission rates of three densities of WFI, a variant of WFI without paraffin wax and EPS were evaluated following ASTM E96, *Test Methods for Gravimetric Determination of Water Vapor Transmission Rate of Materials,* dry-cup method (ASTM International, 2023b). The apparatus used was a straight-sided, circular glass bowl with the samples cut to press fit into the cups. To eliminate the influence of edge width of wax sealing, which is usually applied to the top surface of the sample, on the water vapor permeability of the samples, a modified method was used to assemble the sample. With this method, the edges were sealed with vacuum grease to prevent moisture penetration and press fit into a glass container (Figure 1. 1.) This change eliminated the need to adjust for edge effect in the final results, which is especially critical for these samples given their thickness. As the sample thickness increases, the impact of edge masking errors increases. The samples were conditioned to 21°C and 50% RH until mass reached a constant value, defined as being less than 1% change over 2 hours, and then tested at those same conditions to minimize weight changes resulting from moisture content changes in the material as opposed to moisture transfer into the silica desiccant. Prior to the start of the test, the full assemblies were weighed as a zero-hour measurement. The samples were then placed in an environmental chamber set to 21°C and 50% RH and weighed every 24 hours for 10 days. A standard triplicate was used with a fourth specimen being a blank to determine if any adjustment to the slope was needed for sample weight changes. The weight measurements were plotted, and then the predicted slope from the trendline is used to calculate the water vapor transmission rate (WVTR) (Equation. 1. 2). The relative humidity and a saturation vapor pressure of 2.489 kPa was used to convert WVTR to water vapor permeance (WVP) (Equation.1. 3). The results were adjusted for the permeability of the still

air in the cup (Equations. 1. 4 & 1. 5) and the surface resistance. Permeability was then calculated

by multiplying the WVP by the thickness of the sample (Equation. 1. 6).

$$WVTR = \frac{g}{tA}$$

<div align="right">Equation 1. 2</div>

Where,

g = *Weight change in grams*

t = *Time during which g occurred in hours*

A = *Area of sample surface in* m^2

$$WVP_u = Unadjusted\ Water\ Vapor\ Permeance = WVTR/S(R_1 - R_2)$$

<div align="right">Equation 1. 3</div>

Where,

S = *Saturation vapor pressure at the test temperature, Pa*

R_1 = *Relative humidity in the test chamber*

R_2 = *Relative humidity in the cup*

$$\delta_a = \frac{2.306E-5 * P_0}{R_v * T * P} * (\frac{T}{273.15})^{1.81}$$

<div align="right">Equation 1. 4</div>

Where,

δ_a = *Permeability of still air*

$T = Temperature, K$

P = *Ambient pressure, Pa*

P_0 = *Standard atmospheric pressure, Pa*

$$R_v \; = ideal \; gas \; constant \; of \; water$$

$$Adjusted \; WVP = \; WVP_A = \; 1/WVP_u - \delta_a - SR$$

Where,

$$SR = Surface \; resistance$$

$$Average \; Permeability = \; \delta_A * Thickness$$

Figure 1. 1: Permeability Samples.

2.2.3. Water Retention of WFI

The water retention of the wood fiber insulation was tested following the procedures described in ASTM 1763: *Test Method for Water Absorption by Immersion of Thermal Insulation Materials,* Procedure B (ASTM International, 2020b). The dimensions of the samples were measured at 4

different points using a digital caliper (precision of 0.01 mm) for length and width, and at 12 locations for depth. Finally, they were weighed (precision of 0.01 g) immediately prior to fully submerging them below 12.7 mm of water for 2 hours. The specimens were subsequently removed from the water and allowed to drain on end for 10 minutes. At that point, any remaining surface water was dabbed away with paper towels, and the samples were measured to find the percent water retained as a ratio of the original weight and the original volume. Three different densities of WFI were tested, 110W, 140W, and 180W kg/m^3 (6.87, 8.74, 11.24 lb/ft^3), as well as 140NW and Type IX EPS. Three replicates of each density were tested, these samples were cut from unique panels and retained the factory thickness. The EPS water absorption was measured using Procedure B along with the other samples, despite Procedure C being standard for petroleum-based insulation. This was done to enable a one-to-one comparison of the results under the same methodology.

2.2.4. Thermal Conductivity of WFI

The thermal conductivity of WFI samples was measured by a heat-flow meter (HFM) (HFM M446, Netzsch, Germany) following ASTM C518-21, *Standard Test Method for Steady-State Thermal Transmission Properties by Means of the Heat Flow Meter Apparatus* (ASTM International, 2021a). The HFM measures the thermal conductivity of materials by controlling the temperature on each side of the material with two plates and then measuring the heat flux through the material and using entered values about the materials dimensions to convert the measured heat flux to thermal conductivity, as seen in Figure 1. 2.
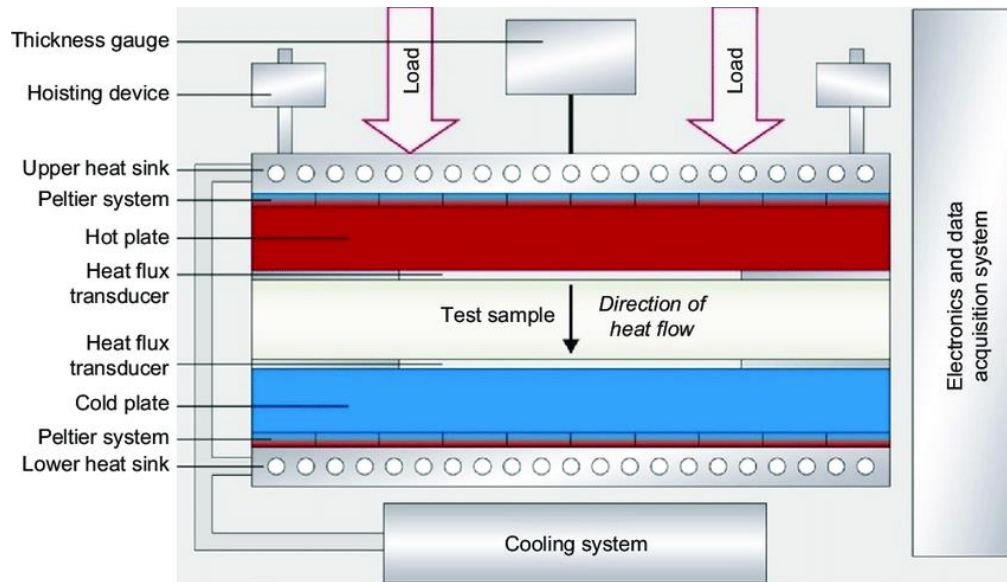
Figure 1. 2: Thermal Conductivity Measurement (Stock, 2021)

Four types of WFI samples (110W, 140W, 140NW, and 180W) were tested to develop a baseline of how the different products would perform. The nominal dimensions of WFI samples were 30.5cm (width) x 30.5cm (thickness) x initial thickness. They were tested at an average temperature of 23.9°C and a delta T of 22°C which are the testing conditions for building envelope materials in a moderate climate stipulated in ASTM C1058 *Standard Practice for Selecting Temperatures for Evaluating and Reporting Thermal Properties of Thermal Insulation* (ASTM International, 2023a). Two replicates were tested for the board at each density, the replicates were cut from unique panels. Each replicate sample was tested twice by flipping and reweighing the sample.

An additional round of testing was conducted using 140NW WFI board and type IX EPS board as a control. This testing was more comprehensive with temperatures ranging from 0-60°C at increments of 11°C and a constant delta T of 22°C. The intent of the experiment was to investigate the correlation of temperature and thermal conductivity of insulation, mimicking the applications

in different climate zones and assemblies, for instance, from freezing to the mid-range of temperatures experienced under asphalt shingles (Winandy 2007, Rose 1992). For each material type, three replicates of each were tested, each being sample tested twice, with the sample being flipped upside down for the second test. The nominal dimensions of samples were 30.5cm (width) x 30.5cm (length) x 10.2cm (thickness). For the hygroscopic WFI board, the samples were placed back to condition in the environmental chamber (21°C and 55% RH) for 24 hours between each test assure that each replicate had the same moisture content at the beginning of each test.

2.3.   Methods for Adhesive Bond Strength Testing of WFI, Lumber, and OSB

2.3.1. Substrate Preparation

Prior to gluing, all substrate surfaces were prepared; a brief summary of the procedures used is provided below. The lumber, NELMA grade 2, was planed in order to guarantee a fresh bonding surface. Both sides of the lumber were planed, removing 1.6 mm from each surface. Planing, instead of sanding, was done in order to keep the pores of the wood open allowing for greater adhesive penetration and an improved bond strength. The lumber was then edged and cut to length, squaring the material and setting the dimensions to 17.8cm x 61.0cm . The WFI and OSB were sanded using a rotary drum sander using 180 grit sandpaper since planing is not a practical option for those materials. Material was removed just to the point that the entire surface was affected by a single pass, <1.6mm. The insulation and OSB were then also cut to 17.8cm x 61.0cm. These initial preparations were performed in batches, guaranteeing that each panel's materials were prepped within an hour of gluing/pressing.

A small hydraulic press was used to fabricate the test samples, Figure 1. 3. A pressure of 455 kPa was selected to minimize the deformation of the WFI while maximizing pressure after an initial

trial in conjunction with one of the adhesive manufacturers was conducted where a small sample of bonded WFI samples were tested for bond strength. For each adhesive we selected the highest recommended spread rate to combat the high absorbency of the WFI. All the manufacturer's recommendations for application were followed and the assembly times for each piece were minimized and kept within the allowance for each adhesive. The primer and water, when applicable, were applied using an aerosolizing paint sprayer, and the adhesives were applied using a squeeze bottle to simulate an extruded resin bead commonly found in commercial manufacturing. Both applications were controlled by placing the substrate on a scale and measuring the added mass of primer/adhesive.

Figure 1. 3: Hydraulic Press Being Used to Fabricate Test Samples.

2.3.2. Bond Strength Test Specimen Preparation

Three test assembly types were made, one with OSB bonded to WFI, one with WFI bonded to lumber, and a third with WFI bonded to WFI, as show in Figure 1. 4. Isolating these three bond lines enabled us to test if any specific bondline within the proposed WIP assembly would pose a problem for the strength of the panel. Two replicate panels were made using each adhesive. After

pressing, the panels were left to set over 24hrs to allow for full adhesive curing. After that time, test specimens were cut from the larger panels. Each panel was cut in half and a random side was chosen to be used for each testing category, shear or tensile. From those halves, six samples were cut, four would be tested and two would be retained as extra specimens in the event that any test materials were damaged or unable to be tested. The tensile testing samples were cut to approximately 5.08cm x 5.08cm following ASTM C209, *Standard Test Methods for Cellulosic Fiber Insulating Board* (ASTM International, 2020a). The samples were affixed to aluminum testing blocks of equal size using a hot melt adhesive. The shear samples were cut to approximately 5.08cm x 3.81cm following ASTM D905, *Standard Test Method for Strength Properties of Adhesive Bonds in Shear by Compression Loading* (ASTM International, 2021b).

Figure 1. 4: Test Panels Prior to Cutting (OSB, WFI, Lumber).

2.3.3. Tensile-Perpendicular to Grain Bond Testing

The tensile-perpendicular to grain, here-after referred to as tensile, bond strength testing was performed following ASTM C209, *Standard Test Methods for Cellulosic Fiber Insulating Board* (ASTM International, 2020a) (Figure 1. 5 left). The testing was conducted using a hydraulic testing frame with a 22.7 kg. calibrated load-cell and a crosshead movement rate of 51 mm/min as required in Section 13.3 of ASTM C209. The samples were mounted to the frame using chains on the top and bottom of the samples perpendicular to the surface allowing the sample to self-align as tension was applied (Figure 1. 5, left).

2.3.4. Shear Strength Testing

The shear strength testing was performed following ASTM D905, *Standard Test Method for Strength Properties of Adhesive Bonds in Shear by Compression Loading* (ASTM International, 2021b). As shown in Figure 1. 5 right, the samples were tested in a guillotine shearing tool mounted to a hydraulic testing frame with a 45.3 kg. calibrated load-cell. The loading rate used was 5 mm/min as required in Section 10 of ASTM D905.

Figure 1. 5: Tensile (left) and Shear Testing (right) Fixture With a WFI:SPF Sample.

3. RESULTS AND DISCUSSION

3.1. Physical and Hygrothermal Properties of WFI

3.1.1. Porosity

The results of the porosity tests conducted on four different types of WFI samples using a gas pycnometer are presented in Table 1. 3. The WFI sample with the lowest density of 110 kg/m^3 had the highest porosity rate of approximately 92%. As the density increased to 140 kg/m^3 and 180 kg/m^3, the porosity rate of WFI decreased to about 90% and 85.6%, respectively. The addition of paraffin wax had a minimal effect on the porosity rate of the WFI samples, as shown in the 140W and 140NW WFI samples. Both 140 kg/m^3 samples have a much higher variability than the other densities. This may be attributable to the vertical density profile, which is consistent for the 110 and 180 kg/m^3 but varies in the 140. The porosity of insulation materials is crucial for thermal conductivity, water retention, water vapor permeability, and structure stability. The influence of the porosity on these properties is discussed in the relevant subsections below.

Table 1. 3: Porosity Results of Four WFI Classes.

WFI samples	Apparent volume, cm^3 (mean±sd)	Skeletal volume, cm^3 (mean±sd)	Porosity, % (mean±sd)
110W	32.02±0.82	2.52±0.04	92.1±0.26
140W	29.26±1.02	2.91±0.19	90.1±1.03
140NW	33.00±3.33	3.11±0.19	90.5±1.63
180W	29.79±0.36	4.28±0.03	85.6±0.17

3.1.2. Water Vapor Permeability Results

The results of water vapor permeability of all specimens after air gap correction are shown in Figure 1. 6. Overall, the four types of WFI specimens tested had much higher water vapor permeability than EPS, which is classified as a water vapor impermeable material (Schiavoni et al., 2016). Increasing the WFI's density resulted in the decrease of water vapor permeability. However, a decrease large enough such that it was statistically different from every other group was only observed when the density was increased from 140 kg/m^3 to 180 kg/m^3; from above 90 ng·s^{-1}m^{-1}Pa^{-1} to 65 ng·s^{-1}m^{-1}Pa^{-1}. Moreover, the porosity results in Table 1. 3 supports this statement because that the porosity of WFI with 110 kg/m^3 was comparable to that with 140 kg/m^3, both of which were greater than that of 180 kg/m^3 by about 6%. As for the paraffin wax treatment, the treatment also caused a decrease in the water vapor permeability but not one large enough for the two populations to be significantly different. The results in this study are comparable with published data (Palumbo, *et al.*, 2016) who reported that wood fiber insulation rigid boards with a density of 210 kg/m^3 and a porosity of 86% had a water vapor permeability of 30 ng·s^{-1}m^{-1}Pa^{-1} (dry cup) and 47 ng·s^{-1}m^{-1}Pa^{-1} (wet cup).
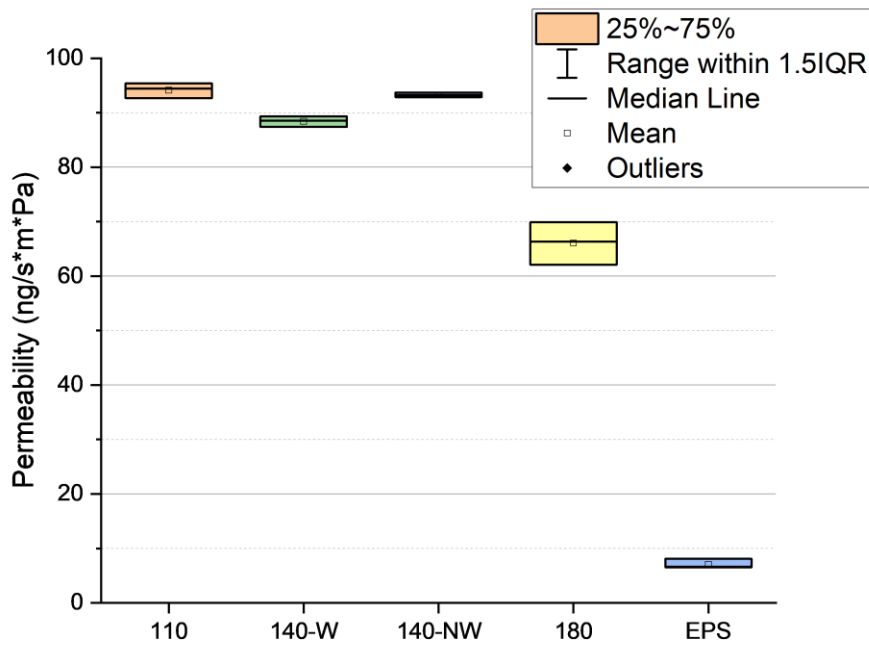
Figure 1. 6: Adjusted Average Permeability of Insulation Samples Grouped by Density.

3.1.3. Water Retention Results

Figures 1. 7 & 1. 8 show the water retention results of several insulation materials (110W, 140W, 140NW, 180W, and EPS as a control) represented two ways, as a ratio of initial weight and as a ratio of initial volume. All the samples were tested under the same conditions. The absorption represented as a percentage of weight ranged from 15-122% across the four WFI variants. The EPS ranged from 25-52% within the sample of three, this variation is likely due to differences in the surfaces of the EPS. A small crack could enable a significant change in the percent difference while not being readily visible. These results are in line with those reported by Muthuraj et al., in 2019. Their study investigated four different bio-based insulation boards, the percent absorption ranged from 20-60% after two hours, with the wood fiber-based panel absorbing 55%, the panels tested did not include any wax but were high density, 454 kg/m^3. The WFI's performance was significantly impacted by the presence or absence of paraffin wax, with a ≈200% increase in both

the weight of water absorbed and the volume of water absorbed for the material without wax. The comparative relationship remained the same between the two metrics apart from EPS. The EPS retained more water on a weight basis than both 110W and 180W but retained the least water on the basis of volume. This variation makes sense given that the EPS has a density as low as 35 kg/m^3. The increase in the 140W as compared to the other waxed WFI products is likely a result of production differences as the different densities are marketed as independent products for differing applications i.e. sarking boards or roof boards, and the 140 kg/m^3 boards had a less consistent vertical density profile than the other products. This testing reveals that the inclusion of wax is critical to WFI's ability to manage bulk moisture, enabling it to perform similarly to petroleum-based insulation products. This reduces the risk of wetting events during or after construction significantly impacting wood fiber insulated buildings, especially when considered in conjunction with the permeability results previously discussed.
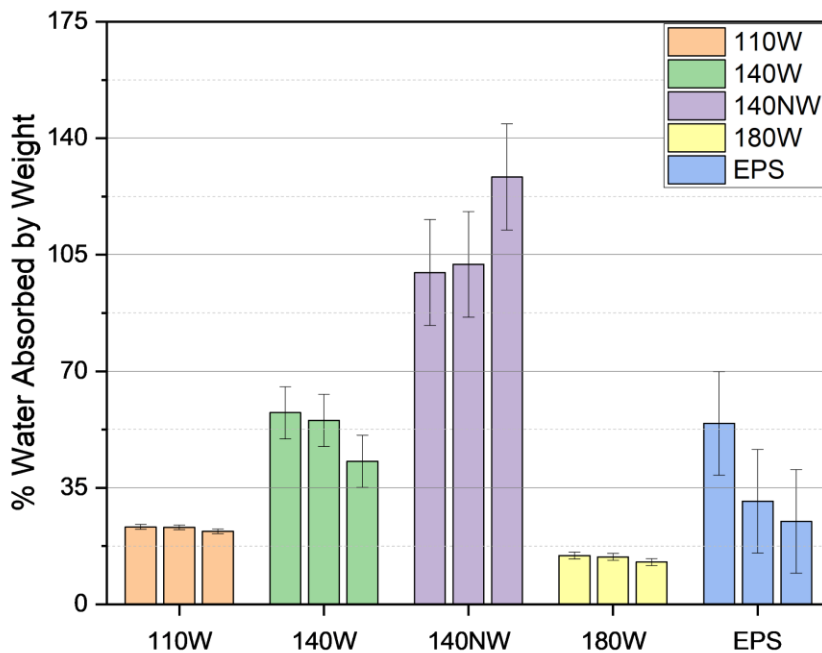
Figure 1. 7: Water Retention as a Ratio of Initial Panel Weight of Various Insulation Materials.
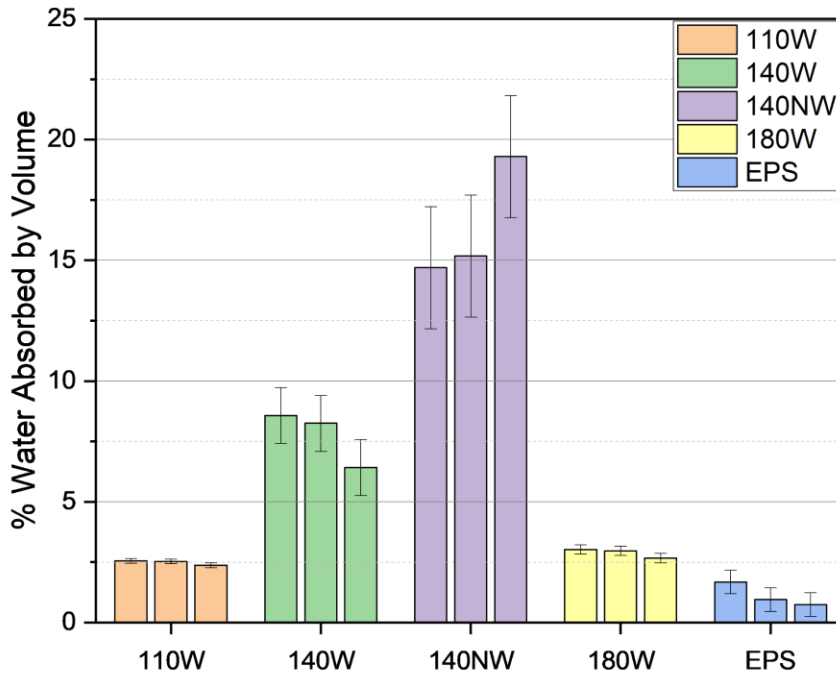
Figure 1. 8: Water Retention as a Ratio of Initial Panel Volume of Various Insulation Materials.

3.1.4. Thermal Conductivity Results

The results of the thermal conductivity testing are displayed in Table 1. 4 as well as Figures 1. 9 and 1. 10. The results in Table 1. 4 show that the material is consistent within its results and has a steady trend of increasing thermal conductivity as the density of the WFI increased. The thermal conductivity went from .038 to .048 (W/(m·K)) as density increased from 110 kg/m^3 to 180 kg/m^3. However, the thermal conductivity mean value of WFI with a density of 180 kg/m^3 was only slightly higher than that of WFI with a density of 140 kg/m^3, indicating the interchangeable use of these two WFI boards. Overall, the thermal conductivity results of WFI samples agree well with previous testing performed by multiple researchers (Cetiner & Shea, 2018; Lawrence et al., 2013; Schiavoni et al., 2016; Veitmans & Grinfelds, 2016).

Table 1. 4: Single Condition Thermal Property Testing per ASTM C518.

Thermal conductivity coefficient (λ), W/(m·K)	WFI samples				EPS samples
	110W	**140W**	**140NW**	**180W**	
Mean	0.038	0.047	0.048	0.048	0.035
SD	1.82E-4	3.29E-4	6.50E-03	1.37E-4	1.02E-04
COV	0.48%	0.70%	13.59%	0.28%	0.30%

Note: All samples were tested at an average temperature of 23.9°C and delta T of 22°C.

WFI is a classified as a hygroscopic insulation material, while EPS is mostly hydrophobic, water is able to occupy space in the pores of the EPS but does not interact directly with the material. The moisture present in WFI (i.e., 6-8% moisture content) in terms of bound water can contribute to the overall thermal conductivity of WFI and alter it as the surrounding temperature fluctuates. Through testing the hydrophobic EPS and hygroscopic WFI for the impact of temperature on thermal conductivity we ended up illustrating two different effects. Figure 1. 9 shows the thermal conductivity results for the WFI. As the temperature increases the insulation becomes less effective relative to the increase in temperature as heat transfers more efficiently through materials as their average temperature increases. (Cetiner & Shea, 2018; Lawrence et al., 2013; Vololonirina et al., 2014) as seen in the beginning of WFI (mean temperatures of 11°C, 20°C, and 30°C) in Figure 1. 9 and throughout the EPS results shown in Figure 1. 10. However, as the temperature rises, a temperature threshold (i.e., the mean temperature of 30°C and delta T of 22°C in this study) is reached where the moisture content of the WFI begins to rapidly decrease, resulting in the rise and

subsequent fall of the thermal conductivity; since in hygroscopic materials, the higher the moisture content, the higher the thermal conductivity (Vololonirina et al., 2014). The moisture content is driven down by the increase in temperature and combats the steady rise of the thermal conductivity related to that same increase in temperature. This effect can be used to justify the implementation of natural insulation materials even in high performance environments where extreme heat is regular. It is important to note that the thermal conductivity of WFI can increase up to 10% and decrease up to 15% before and after the mean temperature surpasses the threshold. Accounting for this change in the energy consumption analysis would lead to a more accurate estimation of energy use when the WFI is used in a building envelope. This would be especially impactful when considering transient energy loads, as the WFI will lose and regain moisture throughout the day as solar gain heats the building and then cools as the sun sets.
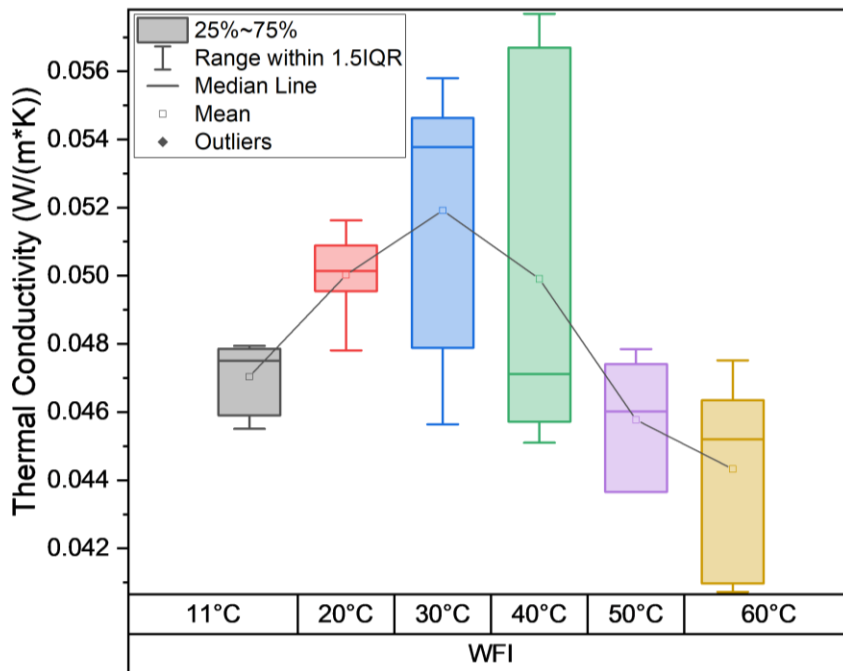
Figure 1. 9: Thermal Conductivity Coefficient of WFI from 11-60°C Mean Temperature.
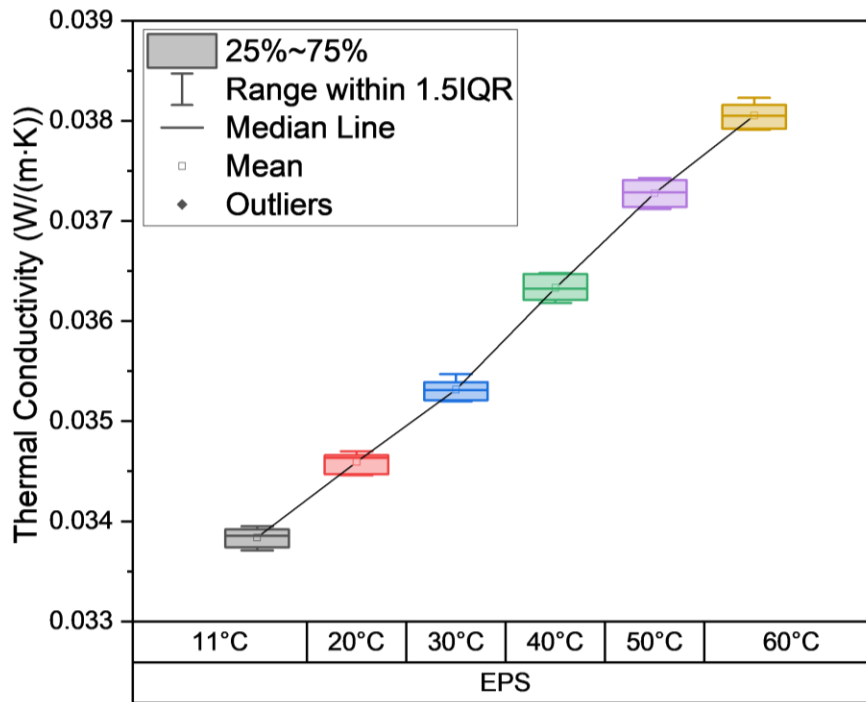
Figure 1. 10: Thermal Conductivity Coefficient of EPS from 11-60°C Mean Temperature.

3.2. Adhesively bond performance of WFI and lumber and OSB

3.2.1. Tensile strength

A box plot of tensile strength results of the nine groups of specimens is shown in Figure 1. 11. It reveals that the mean tensile strength values of all groups were in the range of 10-16 kPa, two of which (WFI:OSB bonded with PUR-R and WFI:WFI bonded with PUR-S) had an outlier with an extremely low value. In addition, the tensile strength results in this study are in line with the data reported by Euring et al. (2015). In that study, the internal bond strength results of two types of WFI boards made of European spruce (*Picea abies*) (200 kg/m³) varied from 9.7 to 20.0 kPa, differing from fiber treatment methods (inactivated laccase-mediator-system in buffer and laccase in buffer) and drying processes (steam-air mixture, hot-air, and hot-air/hot-steam). Further, a two-way ANOVA analysis was conducted to examine the effects of adhesive type and substrate type

on the tensile strength. The statistical analysis results in Appendix B showed that there was a statistically significant difference caused by adhesive type and specimen bond type (p-values of 6.10E-4, and 0.01, respectively). A means comparisons analysis revealed that the means of the WFI:WFI bond was statistically different from the other two bonds, WFI:OSB and WFI:SPF. It also showed that the mean of PUR-S adhesive type was statistically different from PUR-R and EPI. These results can be seen in Appendix B along with the detailed results of the ANOVA.
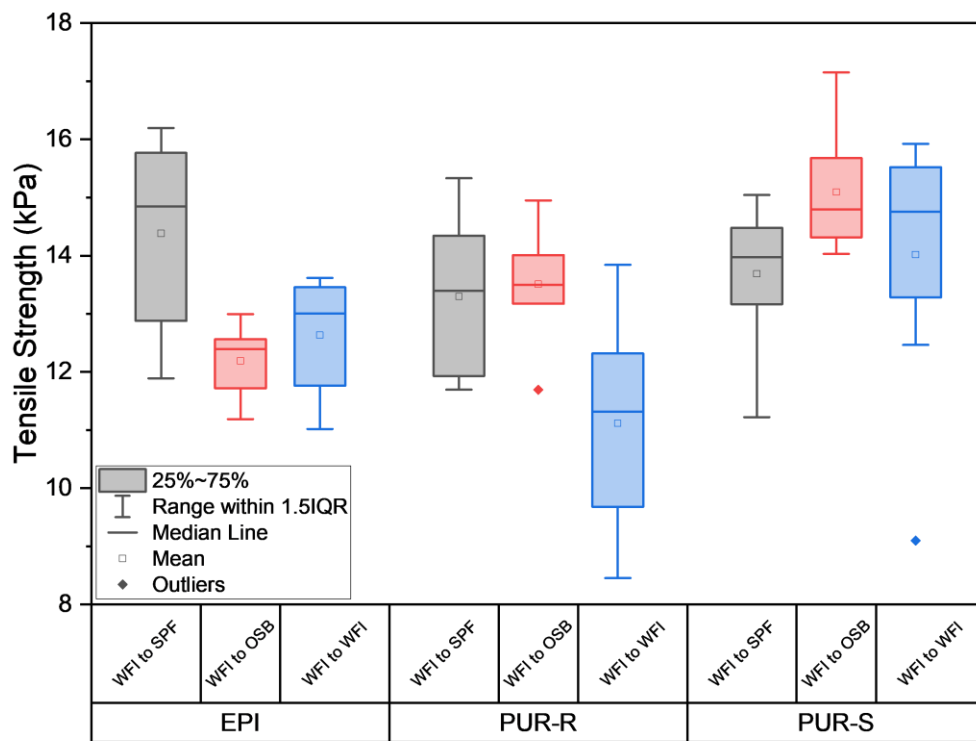
Figure 1. 11: Summary of Tensile Strength Perpendicular to Grain Results.

3.2.2. Shear Strength

The box plot of shear strength results of all the nine groups of specimens is shown in Figure 1. 12. The mean for all nine groupings were in the range of 62-90 kPa Two groupings contained outliers significantly above average (WFI:SPF bonded with PUR-R and WFI:OSB bonded with EPI), these

outliers are a result of the adhesive expanding into the WFI far enough that during loading in the shear fixture the adhesive film was loaded as opposed to the substrates; as a result of this these outliers were excluded from the statistical analysis of the sample. A two-way ANOVA analysis was conducted to examine the effects of adhesive type and substrate type on the shear strength. The statistical analysis results in Appendix B showed that there was a statistically significant difference caused by adhesive type (p-value of 0.04); however, lamina type and the interaction of these two variables was not significant. The mean comparisons analysis revealed that there was no entirely unique group among all the variables tested, when analyzing the interactions between both variables. The only variables that do not share a mean are the PUR-S and EPI adhesives, however, both share a mean with the PUR-R adhesive. These results can be seen in Appendix B along with the detailed results of the ANOVA. A review of the literature did not reveal any existing data related to the shear performance of WFI when loaded in this manner. In-plane shear testing has been investigated on polyurethane-based SIPs, the SIPs had a reported shear strength of 64.25 kPa with the same reported failure modes, all in the core (Kermani, 2006). This data will be crucial in evaluating the feasibility of WIP assemblies applied to walls.
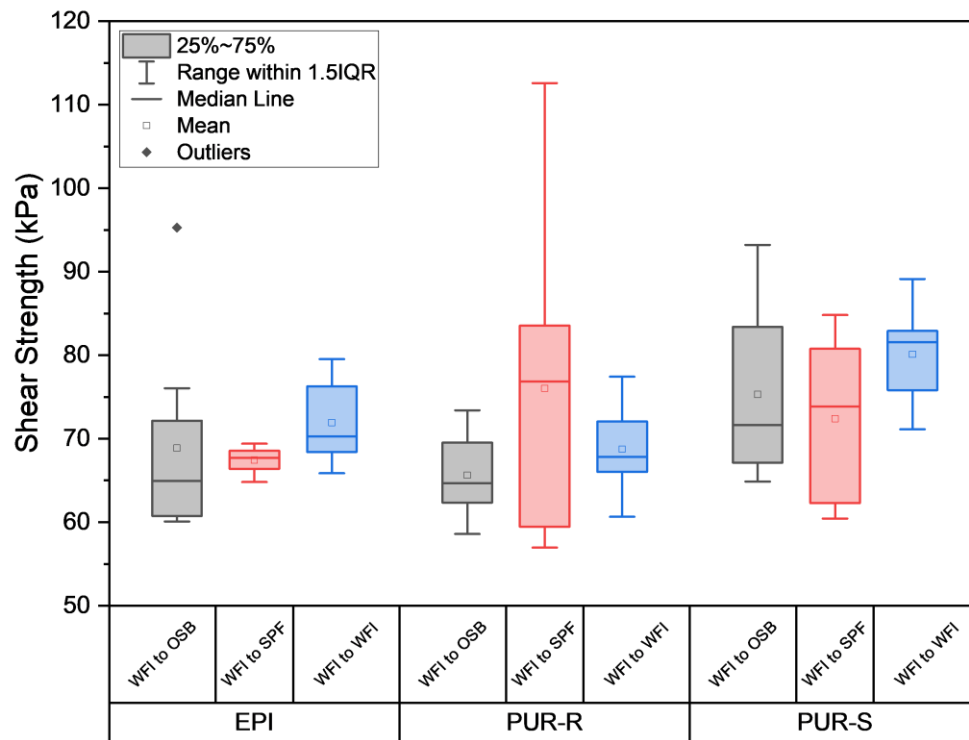
Figure 1. 12: Summary of Shear Strength Results of Specimen Tested.

3.2.3. Failure Mode of Bond Line for Tensile and Shear Strength Testing

The adhesive did not control the strength of the total composite for any of the specimens we tested for tensile and shear strength testing. The 100% wood failure in WFI was observed in all the samples of tensile and shear strength testing. Figure 1. 13 shows the failure mode (i.e., 100% wood failure) of the tensile testing samples. In this study, the adhesive application approach ensured superior bonding performance, regardless of adhesive type and specimen bond type. This was the expected result for this testing as the low-density WFI boards have a very low internal bond strength compared to the other components of WIP panels, e.g., CLT, and OSB. For instance, the internal bond strength of OSB is in the range of 345 kPa to 586 kPa (Zhuang et al., 2022). The

same is true of the shear results, as the samples tested resulted in full wood failure and no adhesive failures.
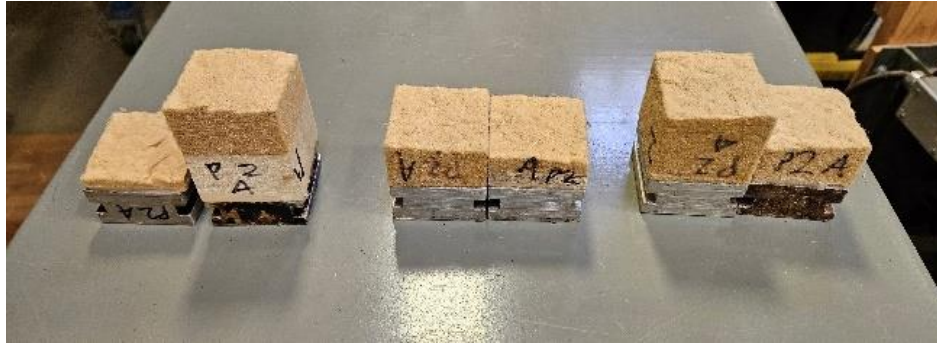
Figure 1. 13: Broken Tensile Test Samples (Left: WFI and Lumber; Middle: WFI and OSB; Right: WFI and WFI).

Based on the testing results, PUR-R was selected for the future optimization of the adhesive application and wood-fiber insulated panel prototype development. The PUR-R is the adhesive that most closely simulates the conditions in a mill where speed will be a critical factor in production.

4. CONCLUSION

In this study, the hygrothermal characteristics of WFI were thoroughly examined to gain an understanding of how these materials would perform, in various climates across the US, as both a wall and roof component, and in the event of major wetting. This understanding is crucial in determining the thickness of insulation required to comply with specific building codes or certifications like PassivHaus while not creating significant risk of mold growth within the building envelope. Furthermore, the bond strength between WFI, lumber, and OSB was tested using three types of structural adhesives, and a PUR adhesive (PUR-R) was chosen for use in the

development of WIP products moving forward. This information will help prevent shear failure and ensure load support requirements are met when determining the total weight of insulation, nail bed, and siding.

Novel all-wood structural panel composites, such as WIPs, offer a compelling answer to the dual-edged problem of addressing emissions in the built environment. WFI has similar or superior properties compared to fossil-based insulation materials that are currently dominating the insulation market in terms of thermal conductivity, structural stability, and moisture management, while also being a carbon sink. The use of adhesives to prefabricate the panels could further reduce the cost of materials and remove the thermal bridging effect of mechanical fasteners. The research findings in this study serve as a baseline for the hygrothermal performance of WFI insulation materials, further research into the performance of the total composite system and the impact of the adhesive layer will need to be performed. Consideration should be given to bio-based adhesive systems as well, given the low strength requirement for the application and the opportunity to further increase sustainability. Critically, the composites must be evaluated for creep behavior, and the impact of the adhesive layer on total assembly permeability as these metrics will critically impact the composites durability in the field. The analysis of these early-stage prototypes will ease the process of industry adoption of these materials, which are a relatively novel introduction to the U.S., and provide a steppingstone for further research in the utilization of bio-based insulation as a mainstream building material.

CHAPTER 2

DEVELOPMENT OF HIGHLY THERMALLY EFFICIENT WOOD-FIBER INSULATED PANELS (WIPS) FOR USE IN BUILDING ENVELOPES: LAB SCALE HYGROTHERMAL TESTING OF WIP PROTOTYPES

1. INTRODUCTION

The built environment is responsible for approximately 40% of global CO_2 emissions per year, equivalent to 14.6 gigatons of CO_2. Out of the total of 14.6 gigatons, 9.9 gigatons are directly related to building operations through heating and cooling (Architecture 2030, 2021). This significant contribution is expected to continue. To achieve the global net-zero emissions targets set by the United Nations by 2050, it is necessary to reduce embodied and operational carbon. Many options for improving the carbon impact of buildings exist: sustainably sourced, low-carbon construction materials, increasing the insulation performance of walls and roofs, improving the airtightness of building envelopes, reducing thermal bridges in building envelopes, installing quality windows and doors, and installing energy recovery ventilation (ERV) systems (see Figure 2.1).
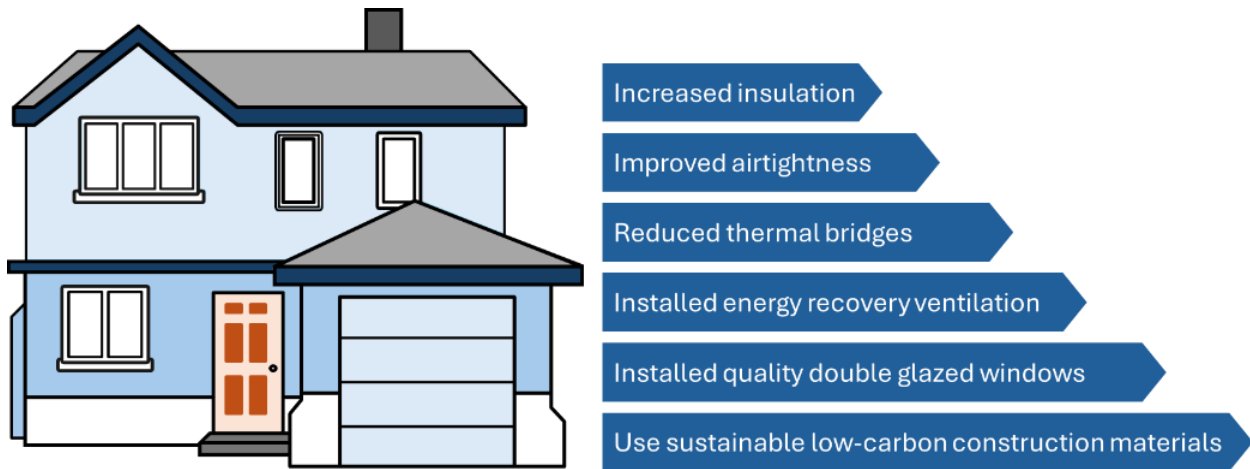
Figure 2. 1: Improvement of Building Energy Efficiency Through Building Envelopes.

Bio-based wood composites, engineered wood products, mass-timber panels, and wood fiber insulations are all examples of building materials with low or negative embodied carbon (see Table 2.1). These materials can be incorporated into a building to improve performance and sequester carbon for the life of the building. Trees act as a carbon sink during growth and then store this carbon in buildings when they are utilized for construction. This carbon sink can be large enough to offset the emissions of harvesting, processing, and installing the wood in buildings, thus allowing a portion of the building to be carbon-negative or neutral. Forest products outperform agricultural residues in this sense; softwood trees forests sequester 7.4 ($MtCO_2e$/yr) of carbon per kg of timber, and harvested forest products retain 4.3 ($MtCO_2e$/yr) after harvest, processing, and installation (Arehart et al., 2021), while agricultural residues, straw, for example, results in a reduction of sequester 3.0 ($MtCO_2e$/yr) when utilized in a structure (Mattila et al., 2012).

Adding insulation to new or existing buildings can be a straightforward and worthwhile means of improving building performance, for example, adding R-2.3 ((m^2*K)/W) insulation to masonry buildings could improve energy efficiency by as much as 65% (Kočí et al., 2020). Prefabricated

insulation panels are gaining popularity attributable to their effectiveness at addressing thermal loss. Furthermore, energy retrofits of existing buildings, as well as new construction, can be done with increased efficiency, decreasing the embodied and operational carbon with one product. However, addressing this issue with petroleum-based insulation materials can be counterproductive because of the embodied carbon of those materials. Polystyrene foam-based insulation materials, a common core for structural insulated panels (SIPs), can have an embodied carbon of 4.2-5.8 kg CO_2 per kg of material (Kunic, 2017) and are formulated using non-renewable hydrocarbon oils. Bio-based wood fiber insulation with a negative embodied carbon, as shown in Table 2.1, is the focus of our study as a replacement for fossil-based insulation.

Table 2. 1: Embodied Carbon of Bio-Based Building Materials and Other Materials

Structural material	Embodied carbon (kgCO$_2$eq/m^3)	Insulation material	Embodied carbon (kgCO$_2$eq/m^3)
Steel Framing[a]	16,400	Extruded Polystyrene (XPS)[a]	25.36
Concrete Block (CMU)[a]	260	Expanded polystyrene (EPS)[a]	2.63
Brick[a]	503	Mineral wool[a]	1.31
North American Lumber[a]	63	Fiberglass Insulation[a]	0.46
North American Glulam[a]	198	Wood fiber insulation (WFI) board[b]	-1.06
[a] Reba, 2022 [b] Wood fiberboard EPD considering the carbon sequestration by trees			

Beyond the addition of insulation, there are many strategies that can increase the efficiency of a building. The climate that the building is in will also inform these strategies. For example, installation of a high-performance cooling system will see significantly reduced returns in a cold climate as compared to a warm one. Improving envelope airtightness could achieve the reduction of annual energy consumption for heating and cooling in low-rise U.S. commercial buildings by 9% to 36%, with the lowest energy saving observed in climate zones 1A (very hot, humid) and 2B (hot, dry) (Emmerich et al., 2007). In addition, minimizing thermal bridges could reduce the annual space heating energy demand by 38–42% for pour-in-place concrete constructions in British Columbia, Canada (Ge and Baba, 2017). Based on simulations generated using EnergyPlus, optimally designed and controlled smart glazed windows installed in buildings could result in up to 18% total building energy cost savings in an ASHRAE medium-sized office building constructed using insulated steel-framed exterior walls (R=13. 5) and a metal roof (R=20.8) in Denver, CO, USA (Lantonio and Krarti, 2022). Application of an ERV system in a two-story office building constructed using insulated concrete exterior walls and plywood floor panels, could result in a reduction of the cooling load by 20 to 30% for the air conditioning system and a decrease of 60-70% for the outdoor air load by the ERV (Fan et al. 2014). In addition, systems beyond building components can have a significant impact on the carbon budget of a building. Examples of this non-envelope driven energy saving strategies include: the use of Energy Star-certified appliances, high-efficiency lighting, smart thermostats, and renewable solar energy. These strategies were not in this study but provide context for the complexities involved in addressing carbon in the built environment.

The focus of this study was solely to develop Innovative wall and roof panels made of wood-based materials that are highly thermally efficient for use in building envelopes. The design concept was to adhesively bond CLT and OSB panels (skin materials) to WFI insulation boards (core material) based on the previous study of *Characterization of Wood Fiber Insulation (WFI) for the Development of Wood-Fiber Insulated Panels (WIPs) for Use in Building Envelope* (Snow et al., 2024). As part of that work, the hygrothermal properties of WFI rigid boards, including porosity, water vapor permeability, water retention, and thermal conductivity, were measured and compared to EPS insulation. The results revealed that the thermal conductivity of WFI insulation (nominal density of 140 kg/m^3) is about 35% higher than that of EPS. In contrast, WFI insulation is more permeable to water vapor compared to EPS. The tensile and shear strength of adhesively bonded WFI and CLT, WFI and WFI, as well as WFI and OSB bonded with three types of structural adhesives (two polyurethane (PUR) adhesives and one emulsion polymer isocyanate (EPI) adhesive), was assessed to identify the potential for scale-up manufacturing of WIPs. The adhesive selected and used for WIP manufacturing in this study was a one-component PUR adhesive with a very short press time of 8 minutes.

The all-wood design of WIPs enables a neutral or negative embodied carbon building component while reducing the mechanical load, i.e., energy demand, on conditioning systems. From the material selection standpoint, wood-based building materials can manage thermal and cooling energy and provide inertia against temperature fluctuations due to wood's intrinsic thermal mass and hygroscopicity. Thermal mass is the multiple of the material density and its specific heat capacity, or the amount of energy required to heat the unit volume of material one degree. Wood has a specific heat capacity of 1.70 (kJ/kg*K) at a density of 470 kg/m^3 and 12% moisture content,

and a thermal conductivity of 0.116 (W/(m*K)) (Forest Products Laboratory, 2021) (FPInnovations, 2013). This combination of properties enables massive wood structures to reduce the interior space's mechanical conditioning (i.e., HVAC) requirements. This effect is achieved by storing thermal energy in the material; the heat is then released slowly as exterior temperatures drop, buffering the diurnal temperature changes. A building energy model was used to compare a mass-timber building with a light wood frame building, beyond the construction method, all other inputs remained the same (occupancy, mechanical systems, insulation level, etc.). The model showed that a light frame wood building had greater heating and cooling demands, illustrating that the thermal mass of the mass-timber resulted in energy savings for all climate zones. The highest impact, a conditioning energy savings of 25% after 14,000 heating and cooling days, was seen in a mixed climate with both heating and cooling days (FPInnovations, 2013). Another study comparing CLT walls to light-frame wooden walls measured an overall energy savings of 22% depending on the climate zone (Salonavaara et al., 2022). This capacity for heat storage can be designed for in the insulative layer as well as the structural components. Wood fiber insulation has a specific heat capacity of 2.10 (kJ/kg*K) at a density of 140 kg/m^3 and a thermal conductivity of 0.040 (W/(m*K) (Steico, n.d.). Comparatively, EPS has a specific heat capacity of 1.45 (kJ/kg*K) at a density of 25 kg/m^3 and a thermal conductivity of 0.036 (W/(m*K)) (Rüdisser, 2018). Further, given the much higher density of the WFI, a significantly higher weight of material will be installed in the building. This enables more benefits to be derived from the natural structure of the wood than just heat storage as well.

Similar to managing temperature through thermal mass, wood-based materials, including CLT, WFI, and oriented strand board (OSB), have the ability to absorb and release moisture at average occupancy temperatures and relative humidities through porosity and hygroscopicity. This enables

37

the wooden structure to moderate spikes in relative humidity perceptible to the occupants, reducing the load on mechanical conditioning equipment and improving occupant comfort (Forest Products Laboratory, 2021). The moisture absorbed during spikes is then released during any humidity drops, reducing the need for mechanical conditioning at both high and low humidity. This buffering effect has been shown to reduce the amount of time in uncomfortable relative humidity conditions in a CLT building by 46% (Salonavaara et al., 2022). Building materials that are not hygroscopic lack this ability to buffer moisture in the indoor environment, and without conditioning equipment to manage the indoor environment, occupant comfort may be negatively impacted.

Improving the insulative factor of a building envelope by minimizing thermal bridges, e.g., repeating thermal bridges (i.e., framing), linear thermal bridges (i.e., junctions at two elements), and point thermal bridges (i.e., mechanical fasteners) can vastly improve the operational carbon budget of a building. Repeating thermal bridges are present in every light frame building and can significantly reduce the overall insulative performance. Christensen (2010) characterized the impact of repeating thermal bridges in light frame construction as a reduction of 3-12% in the R-value of the building using finite element modeling. Variation in this percentage was driven primarily by the framing factor or the percentage of the overall wall made up of studs. Linear thermal bridges are continuous, non-repeating paths through which heat can flow. The most common example of a linear thermal bridge is the connection of a wall element to a floor element in either light or heavy frame construction. One study investigating four different wall construction materials, prefabricated concrete panel, brick, wood (log), and autoclaved aerated concrete, found that linear thermal bridges can account for 23-34% of all heat flow through a building depending on the insulative performance of the wall components (Ilomets et al., 2014). Point thermal bridges are present in any building component that is composed of sheet materials fastened together with

mechanical fasteners. Some less impactful examples are fasteners for sheathing materials and fasteners for siding. Point thermal bridging is of most concern when the primary insulation of a building is a continuous exterior envelope fastened to the building by large fasteners that penetrate the entire insulative layer; this can increase the U-value of the envelope anywhere from 13-35% (Sadauskiene et al., 2020). The fastener schedule, i.e., density is a critical factor in this effect, as well as the thickness of the insulative layer. A study investigating the impact of mechanical fasteners on aero-gel insulation boards used as a continuous exterior envelope found that the fasteners reduced the insulative value of the wall design by 13% using a fastener density of three fasteners per square meter. That value more than tripled to 45% at six fasteners per square meter (Berardi & Ákos, 2019). Additionally, point thermal bridging can present a problem for retrofit applications when insulated facades are installed to increase thermal performance. Finite element modeling has been used to simulate mineral wool and aluminum cladding systems and investigate the impact of thermal bridging in this system. The study found that a reduction of 5-20% to the R-value of the system was expected, depending on the insulative performance of the structural wall and the air gap between the cladding and insulation (Theodosiou et al., 2015). The WIP design reduces the effect of thermal bridging by employing large-size CLT panels, WFI boards, OSB panels, and adhesive bonding techniques to drastically increase the thermal performance of highly insulated wall systems.

The adhesive bonding technique used in WIP manufacturing lends itself well to pre-fabrication, which can further reduce the embodied carbon of the building attributable to the increased manufacturing efficiency related to increased automation. This, in turn, decreases construction time and reduces waste on job sites. Construction time is directly correlated to a building's carbon

footprint, as much of construction emissions are related to equipment idle times as they are waiting for the previous step in construction to be completed (Akbarnezhad et al., 2017). Data collected on construction equipment in 2005 showed that construction activities accounted for 32% of all land-based non-road nitrogen oxide emissions and 37% of land-based particulate matter (US EPA, 2006). Additionally, Guggemos et al. (2006) reported that equipment uses accounts for 50% of most types of emissions and energy use during construction processes. Two of the highest emitting pieces of diesel-burning equipment on a job site, a crane (26.57 kg CO_2/hour) and generators (62.93 kg CO_2/hour), can have operational time cut by increasing the efficiency with which buildings are constructed (Tang et al., 2013). Cranes have especially significant idle times on traditional high-rise construction sites that can be directly reduced by introducing prefabricated elements. Prefabricated elements have specifically been investigated for their impact on the embodied carbon budget of buildings. One study reported that life cycle assessment (LCA) models predict greenhouse gas emissions of 336 kg/m^2 for prefabricated components and 368 kg/m^2 for conventional construction, a reduction of 9% overall. When that reduction is separated into its component factors, it results in an 86.5% reduction in greenhouse gas emissions related to the embodied carbon of the materials, an 18.3% reduction related to construction equipment, a 10.3% reduction associated with the transportation of waste, and a 0.2% reduction related to the transportation of soil (Mao et al., 2013).

In summary, the WIP design offers extremely high hygrothermal performance while reducing embodied carbon and operational carbon emitted over the lifetime of the building. The WIP could easily be prefabricated offsite, offering further benefits to the embodied carbon of the built environment. Additionally, there is a large potential market for products addressing operational carbon emissions of existing buildings, as many of the U.S. buildings manufactured before 1970

are under-insulated or completely uninsulated (Levy et al., 2016). Creating a product that addresses this issue, is convenient, and is rapidly deployable could be a major combatant in the fight against carbon emissions. Furthermore, new construction will continue indefinitely with increasing populations across the globe, and interest in sustainable materials continues to develop every day. Towards this end, the following goals and objectives were identified as most relevant:

- Design and manufacture three different forms of highly thermally efficient CLT walls:

  (a) A WIP where lamina, including WFI, were adhesively bonded together (Assembly A),

  (b) A mechanically fastened WFI wall (Assembly B) and

  (c) A mechanically fastened EPS insulated wall (Assembly C).

- Assess the hygrothermal performance of three CLT panels by conducting lab-scale testing in a simulated cold environment.

- Assess the adhesive's impact on moisture and the wall assembly's thermal properties.

2. MATERIALS, WIP PANEL DESIGN, AND INSTRUMENTATION

2.1. Panel Materials

2.1.1. CLT and OSB as Structural Substrates

The 3-ply CLT used in this study was sourced from a European manufacturer and cut from a larger billet into the components used. The CLT was manufactured using a commercial mix of European spruce species. The moisture content of CLT samples was measured as $11.70 \pm 0.60\%$ (mean±SD), and the density was 337 ± 6 kg/m^3 at the listed moisture content.

OSB panels were sourced from a local retailer. The OSB was manufactured with Southern yellow pine wood strands, polymeric methylene diphenyl diisocyanate (pMDI) adhesive, and wax to

manage moisture. The OSB used in this study had a nominal thickness of 1.59 cm. The moisture content of OSB was $9.80 \pm 0.20\%$ (mean±SD), and the corresponding density of the OSB was 601 ± 20 kg/m^3 at the listed moisture content.

2.1.2.WFI and EPS Insulation

Table 2. 2: Summary of Crucial Panel Substrate Physical Properties.

Materials	Nominal Density (kg/m^3)	Thermal Conductivity (λ) W/(m·K)	Permeability (ng/s*m*Pa)	MC %	Thickness (cm)
WFI	140	0.048[A]	93.29	7.5[B]	10.20
EPS	30	0.035[A]	7.09	N/A[B]	5.08
					10.16
OSB	600	0.137[A]	0.65	9.8[B]	1.59
CLT	340	0.116[A]	1.83	11.7[B]	10.32

A: At 21°C
B: Prior to the experiment

The WFI materials used in this study were sourced from a European manufacturer and made using a dry process. The boards were formulated from dry softwood fibers and pressed into boards after a mix of adhesive and other additives; often, water repellants or fire retarders are sprayed onto the dry fibers as part of the production process. The WFI boards were manufactured with pMDI, and the boards had paraffin wax as an additive to reduce the water uptake (De Ligne et al., 2022; Kirsch et al., 2018). WFI is a hygroscopic and vapor-permeable material with a permeability of 93.29 (ng/s*m*Pa) (Snow et al., 2024). The panels had a measured density of 148.78 ± 1.40 kg/m^3, which was slightly higher than the nominal density by 6.40%. The panels were 10.20 cm thick. The

moisture content of WFI panels upon construction of the wall components was within the range of 7% to 9%, see Table 2.2.

The EPS insulation used was purchased from a domestic supplier. The EPS was specifically type IX EPS with a density of 30.40 ± 0.60 kg/m^3. Boards of two different thicknesses were used, 5.08 cm and 10.16 cm, to achieve a similar design R-value to the other assemblies. EPS is a hydrophobic and semi-vapor permeable material with a permeability of 7.09 (ng/s*m*Pa) (Snow et. al., 2024).

2.1.3. Fasteners and Adhesives

Stainless steel structural screws were used to assemble two of the wall designs, the traditional WFI wall and the EPS wall. The length of both screws was selected such that they would penetrate the second laminae of the CLT after passing through a furring strip and two layers of insulation. The screws were manufactured using 304 stainless steel and had an area of 0.25 cm^2 in assembly B and 0.28 cm^2 in assembly C. The fastening pattern of the screws was such that four screws were installed per square meter of the wall, spaced 40.6 cm in the center horizontally and 61.0cm in the center vertically. The adhesively-bonded WIP components were laminated using a rapid-set single-component polyurethane (PUR) adhesive commonly used for SIP manufacturing, which was identified by Snow et al. (2024).

2.1.4. Water and Air Sealing

The wall assemblies included weather-resistant barriers so that moisture relations observed within the wall would be similar to those observed in situ. Solitex Mento 3000 was used for assemblies B and C; this membrane was used for these two assemblies because of its use in the in-situ assembly that control A represents. The Solitex Mento 3000 has a stated vapor permeance of 3298.90 (ng/s*m^2*Pa) (Pro Clima, Schwetzingen, Germany). Assembly A used Tyvek Home wrap; this membrane was selected for use in this assembly based on its prominence in domestic

applications when siding is attached directly to a nailbed substrate. The Tyvek Home wrap has a

stated vapor permeance of 3089.50 (ng/s*m^2*Pa) (Dupont Tyvek Construction, Delaware, USA).

Impermeable flashing tapes were used to wrap the perimeter of the assemblies prior to testing,

leaving only the interior and exterior wall faces exposed prior to installation in the test set-up. This

was done to prevent moisture from traveling in or out through the assemblies except through the

wall faces. Protecto Wrap sill pan flashing and 3M 8067 all-weather flashing tape were used on all

assemblies. The sill flashing was a polyethylene tape with rubberized asphalt adhesive, and the all-

weather flashing was an elastomeric tape with pressure-sensitive acrylic adhesive. Both flashing

products are stated to be impermeable to water vapor.

2.2. Wall Panel Design

All assemblies of type A, B, and C are 60.96 cm x 60.96 cm with varying thicknesses depending

on the combination of substrates and insulation. Diagrams of all three assemblies can be seen

below in Figures 2.2 – 2.4. The photos of all three assemblies are listed in Figure 2.5.
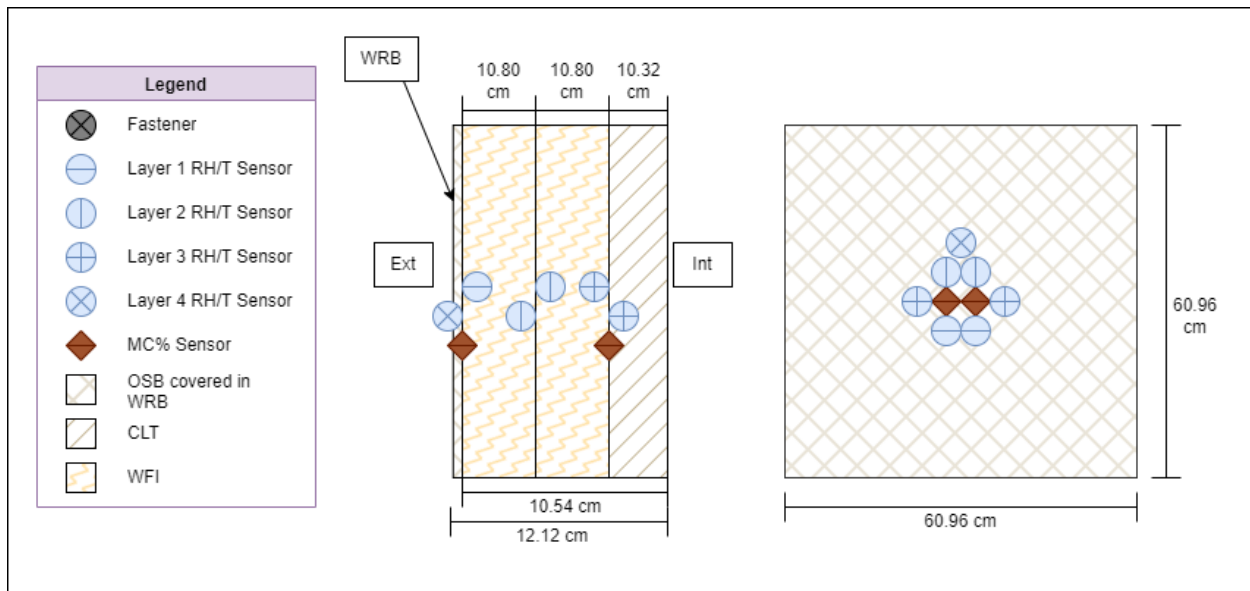
Figure 2. 2: Assembly A Diagram.

44
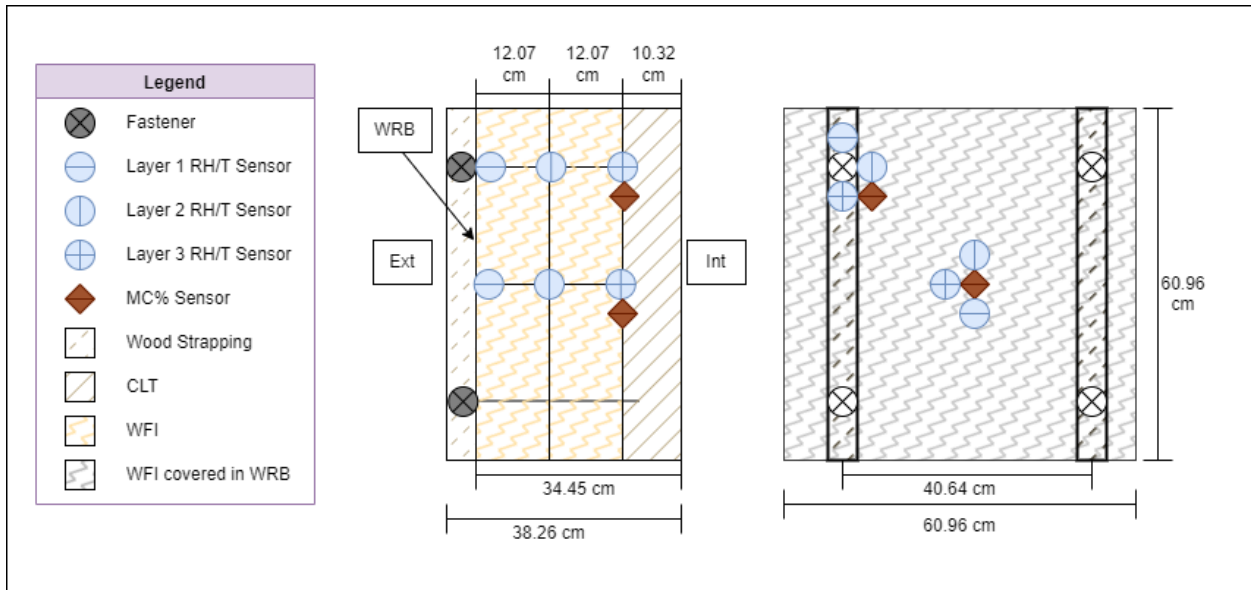
Figure 2. 3: Assembly B Diagram.
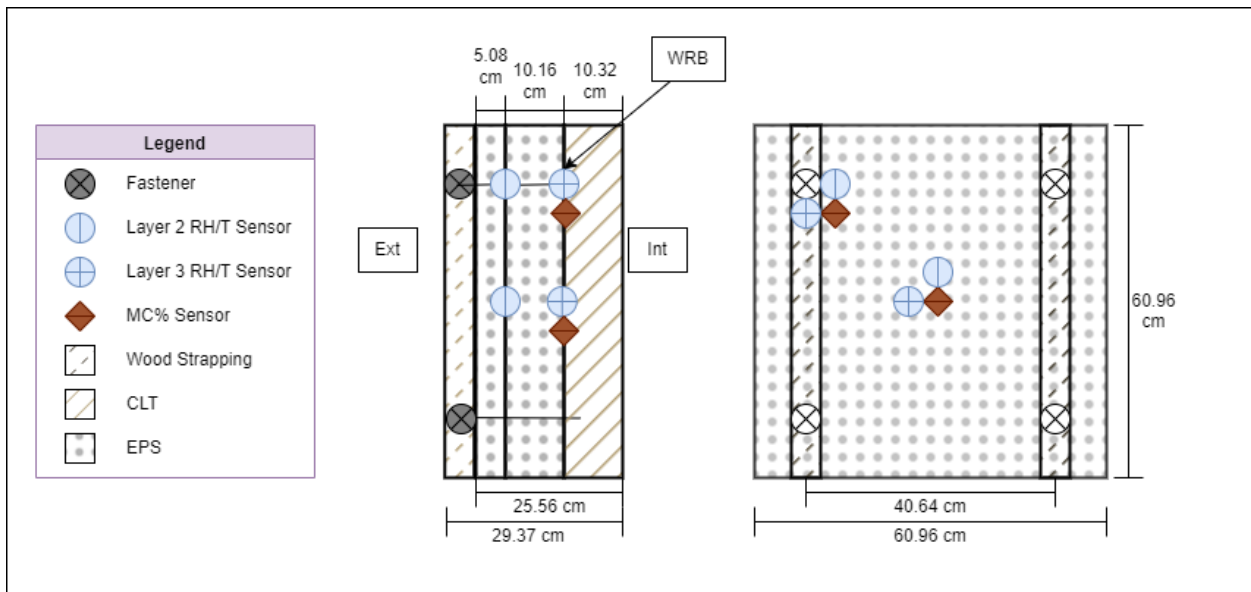
Figure 2. 4: Assembly C Diagram.

2.2.1.WIP Assembly A: WFI adhered with structural adhesive

In Assembly A, a sheet of 1.59 cm OSB was adhered to the exterior face of the WFI, using a rapid set foaming polyurethane adhesive that is commonly used for SIP construction by existing manufacturers. This OSB acted as a nailable substrate for the attachment of the WRB, Tyvek,

which was stapled to the OSB. An adhesive deposition rate of 215 g/m^2 was used for each bondline and the adhesive was applied in beads spaced 1.9 cm apart along the length of the wall components. The pressure and pressing time used were described by Snow et al. (2024).

2.2.2. Assembly B: WFI with mechanical fasteners

The design of control Assembly B was chosen to reflect an existing building constructed in Belfast, ME. Assembly B followed the same CLT and WFI layout as Assembly A. However, the exterior surface of the wall component differed. Two layers of the WFI insulation were placed directly against the CLT, with a WRB, the Pro-Clima 3000, placed exterior to the insulation and CLT. Furring strips were installed exteriorly on the entire assembly, and the mechanical fasteners were driven through all layers and into the second laminae of the CLT.

2.2.3. Assembly C: EPS with mechanical fasteners

The design of control Assembly C reflected standard construction methods when using EPS as a continuous exterior thermal barrier. In this case, the CLT was wrapped with a weather-resistant barrier (WRB), Pro-clima 3000, to manage bulk moisture. Two pieces of EPS insulation were placed exterior to this barrier, one 5.08 cm piece and one 10.16 cm piece. Furring strips were then placed on the exterior of the insulation, and the mechanical fasteners were driven through all layers into the second laminae of the CLT.

Table 2.3 summarizes the three assembly designs. All prototype wall assemblies were designed to target a nominal total R-value of 6.00 m^2·K/W, within the limitation of using readily available insulation thicknesses. For instance, the total R-value of Assembly C (EPS insulation) was about 5.4 m^2·K/W, while that of Assembly A (WFI insulation) was about 6.20 m^2·K/W.

Table 2. 3: Summary of Assembly Designs.

Assembly	Components				Attachment	Total thickness	Design total R-value, m²·K/W
	CLT, 3-ply	Insulation	OSB	WRB			
A	10.16 cm (thickness)	WFI, 21.75 cm (thickness)	Y	Tyvek	Adhesive	35.88 cm	5.67
B		WFI, 24.13 cm (thickness)	N	Pro-Clima	Fasteners	34.29 cm	6.06
C		EPS, 15.24 cm (thickness)	N	Pro-Clima	Fasteners	25.40 cm	5.41

Figure 2. 5: Lab-Scale Components in Various Stages of Construction

Assembly A (left), Assembly B (center), Assembly C (right).

2.3. Instrumentation for Hygrothermal Performance Assessment

2.3.1.RH/T Sensors, MC Sensors, and Data Logger

Omni-sense A-1 HumiSense temperature and humidity sensors were used to monitor relative humidity and temperature throughout the samples. The sensor units consisted of a 5 mm diameter probe cabled to a 3.5 mm TRRS audio plug. The sensors can read temperatures of -40 to 120°C

and 0-100% RH. The sensors have accuracies of $\pm$ 0.3°C and $\pm$ 2.0% RH at the optimal temperature range of 10-60°C.

Omni-sense A-2 wood moisture content sensors were used to monitor MC % at several points of the CLT panels. The sensor consisted of two leads ending in ring terminals that were affixed to the CLT by stainless steel screws 19.05 mm long. A calibration of these sensors was conducted before doing the lab-scale experiment. Paired wood blocks cut from CLT panels were conditioned at three RH levels, 50%, 75%, and 90% at room temperature, in an environmental chamber until reaching an equilibrium status, which created the corresponding MCs of wood are 9.5%, 14%, and 20%, respectively based on the sorption isotherm (Forest Products Laboratory, 2021). The laboratory oven-drying method was used to obtain the accurate MC of the wood blocks after conditioning following *ASTM D4442-20 Standard Test Methods for Direct Moisture Content Measurement of Wood and Wood-Based Materials* (procedure B) (ASTM International, 2020), while their MCs were measured using the sensor. The results were compared to measured data of spruce blocks and the oven-dry moisture content of co-located blocks, and a correction factor of – 1.5% wood MC was found to be adequate. The calibration data are summarized in Appendix A. It is noted that the MC sensors were not compatible with the WFI because of the low density of the material. This results in an inconsistent connection between the electrical contacts and the insulation, making electrical resistance measurements in the composite unreliable.

Data from the sensors were collected using Omni-sense's integrated data management platform. The data were collected with S-2 wireless data loggers set to take readings from all Omni-sense sensors every five minutes. These data were then uploaded to the Omni-sense cloud storage site via the G-4 wireless gateway. All Omni-sense components are shown below in Figure 2.6.

2.3.2. Heat Flux and Data Acquisition

Hukseflux HFP01 heat flux sensors (HuksefluxUSA, Inc. 15 Frowein Road, Suite E-3, Center Moriches, NY 11934, USA) were used to measure the actual heat flux through the wall assemblies in order to confirm the designed values for the total R-value of each wall system and assess the heat loss through the thermal bridge created by the steel screws in Assembly C (Figure 2.7). The sensors had a measurement range of ± 2000 W/m^2 in a temperature range of -30 to 70°C. Each sensor contained a thermopile that produced a voltage reading at a given heat flux; the manufacturer provided each sensor with a sensitivity rating to convert the voltage to heat flux; the nominal sensitivity was 60 x 10^{-6} (V/(W/m²). All sensors were calibrated by the manufacturer and had an uncertainty of $\pm$ 3%. Sensors were placed on the exterior of every panel (i.e., cold surface) at the center point of the wall area. Sensors were also placed near screw locations in Assembly C to measure the influence of the penetration on the overall system. The sensors were installed in compliance with *ASTM C1046-95: Practice for In-Situ Measurement of Heat Flux and Temperature on Building Envelope Components*. Voltage data from the heat flux sensors was collected using two OM-CP-OCTPRO data loggers.

Figure 2. 6: Omni-Sense Probes and Data Logger.

Figure 2. 7: Hukseflux Heat Flux Sensor.

3. METHODS

3.1. Experiments for Hygrothermal Performance Assessment

3.1.1. Test Set-Up

Two replicates of each wall assembly design were manufactured, and then the six panels were fashioned together to form a test cube (see Figure 2.8). This experimental design allowed for the control of the temperature on each side of the wall once the whole assembly was placed inside an environmental chamber. Temperature/RH sensors and wood moisture content sensors were placed

throughout the wall panels' thickness to monitor the diffusion of heat and moisture. The same temperature/RH sensors were placed throughout the interior and exterior of the cube to monitor the conditions at the surface of the walls as well as air temperature and RH. The primary point of interest was the center of the wall area at each lamination interface; data collected at the center of the wall areas was used as the primary comparison between wall assemblies, replicates, and other points of interest. Data collected at these points were the least likely to be affected by boundary conditions, isolating movement of moisture and temperature through the assembly from interior to exterior. The exterior boundary conditions are not entirely isolated however, the depth of the wall assemblies is exposed to the lower temperatures, so 3-dimensional heat flow is still occurring if limited. Another point of interest was the penetration point of the mechanical fasteners (Assemblies B and C); the same sensor schedule used at the center of the walls was replicated at a fastener penetration point to monitor the effect of the mechanical fasteners. The final point of interest was the interphase created by the adhesive bond in the WIP panels. In order to quantify its impact, sensors were co-located in the center of the wall on both sides of the adhesive barriers. Models of the instrumentation scheme are shown below in Figure 5. Data were collected from January to August 2023.
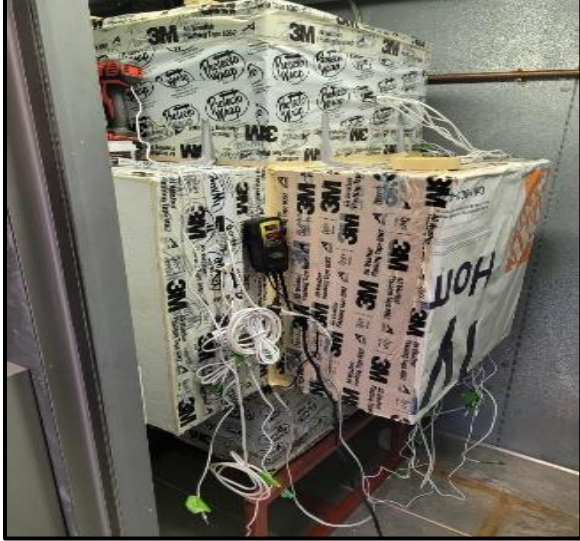
Figure 2. 8: Test Cube Formed by Six Assembles in An Environmental Chamber.

3.1.2. Environmental Chamber and Conditions

A Norlake Scientific walk-in environmental chamber maintained the simulated exterior environment. The temperature of the chamber (the cube's exterior) was set to 0°C in order to simulate a winter day in Maine, at this setpoint the chamber only reached 5°C. The target interior temperature of the cube was set at 21°C and maintained by a small non-directional ceramic heater in conjunction with a small fan circulating air inside the cube. This temperature was not achieved at all times and locations throughout the experiment.

The relative humidity (RH) was uncontrolled inside and outside the test assembly. The RH in the chamber fluctuated with the climactic conditions in Maine, moisture was able to rise and fall naturally and the RH inside the test assembly responded to the same environmental changes. This allowed data to be collected assessing the CLT's MC% changes over the testing period without the influence of artificially supplied water vapor.

3.1.3. Calculation of Total Thermal Resistance and Point Thermal Bridge Adjustment

The thermal resistance of the assemblies tested was calculated using Equations 2.1 – 2.3, per ISO 6946: 2017 *Building components and building elements: thermal resistance and thermal transmittance calculation methods* (ISO, 2017). The calculations provide estimations for the total R-value as well as the impact of point thermal bridges introduced by mechanical fasteners that penetrate the insulative layer of a building component. A ΔU factor is calculated based on the fastener schedule and the characteristics of a given fastener. This factor is then subtracted from the overall predicted U of the component, resulting in an adjusted insulative value. These reductions are later compared against the measured increase in heat flux at a fastener penetration.

Equation 2.1. ISO 6946: 2017 Simplified calculation of thermal resistance

$$R = \frac{d}{\lambda}$$

Equation 2. 1

Where,

d = Depth of material (m)

λ = Thermal conductivity of material (W/(m*K))

Equation 2.2. ISO 6946: 2017 Simplified calculation of total thermal resistance

$$R_{total} = R_{si} + R_1 + R_2 + \cdots + R_n + R_{se}$$

Equation 2. 2

Where,

R_{si} = Internal surface thermal resistance ((m^2*K)/W)

R_n = Thermal Resistance of each component layer ($(m^2*K)/W$)

R_{se} = External surface thermal resistance ($(m^2*K)/W$)

Equation 2.3. ISO 6946: 2017 Simplified calculation of point thermal bridging effect:

$$\Delta U_f = \alpha \times \frac{\lambda_f \times A_f \times n_f}{d_I} \times \frac{R_I}{R_{total}}$$

Equation 2. 3

Where,

ΔU_f = Adjustment to the total U of the wall assembly ($W/(m^2*K)$)

α = A constant provided by ISO 6946: 2017 (See Table 5)

λ_f = Thermal conductivity of fastener material ($W/(m*K)$)

A_f = Area of a single fastener (m^2)

n_f = Number of fasteners per square meter

d_I = Depth of insulation (m)

R_I = Thermal resistance of insulation ($(m^2*K)/W$)

R_{total} = Thermal resistance of total assembly ($(m^2*K)/W$)

The material parameters and thermal properties for the calculations are listed in Section 4.4.

4. RESULTS AND DISCUSSION

4.1. Environmental Conditions

The conditions measured within and outside of the test cube are shown in Figures 2.9 and 2.10 below. The temperature varied a maximum of ±2.5°C from one position to another inside the actual test cube. By comparing the actual temperature measured at each location with the target temperature of 21°C, the most significant variation, approximately 22°C, was measured at the top center, while all other positions were within 2°C. The temperature within the chamber was maintained at a reasonably constant level with little to no fluctuation. The replacement of a malfunctioning heating element caused the temperature change that occurred in March. The spikes seen in all the figures were caused by either unplanned power outages or times when the chamber had to be opened to assess the assembly.

The relative humidity (RH) in the chamber and within the test cube showed natural daily and seasonal fluctuations (Figures 2.9b and 2.10b). The low RH interior and high RH exterior align with the conditions that would be experienced in a home in the Northeast or other mixed winter climate zones. This results from the outside air having a low capacity for moisture, given its low temperature. When the air was heated in the interior space, the capacity for moisture was increased, but the amount of moisture in the air was not increased due to a lack of additional humidity supply. This resulted in the drying of CLT panels and a consistent moisture differential in the wall assemblies.

The vapor pressures, the pressure exerted by the concentration of moisture in the air of a given space, are shown below in Figure 2.11. For water vapor to pass through a barrier there must be a pressure differential between the two locations. However, moisture levels can still be affected by hygroscopic materials without the need for a pressure differential on each side of the material

because the moisture is being taken up by the material itself that is either binding the water to itself or taking it into pores that have their own pressure differentials. It can be seen that the interior and exterior pressures begin to equalize in May 2023. This corroborates the changes, or lack thereof, in RH presented in the following sections as water vapor would not be driven in either direction.

(a) Temperature profiles of five locations in the test cube

(b) RH profiles of five locations in the test cube
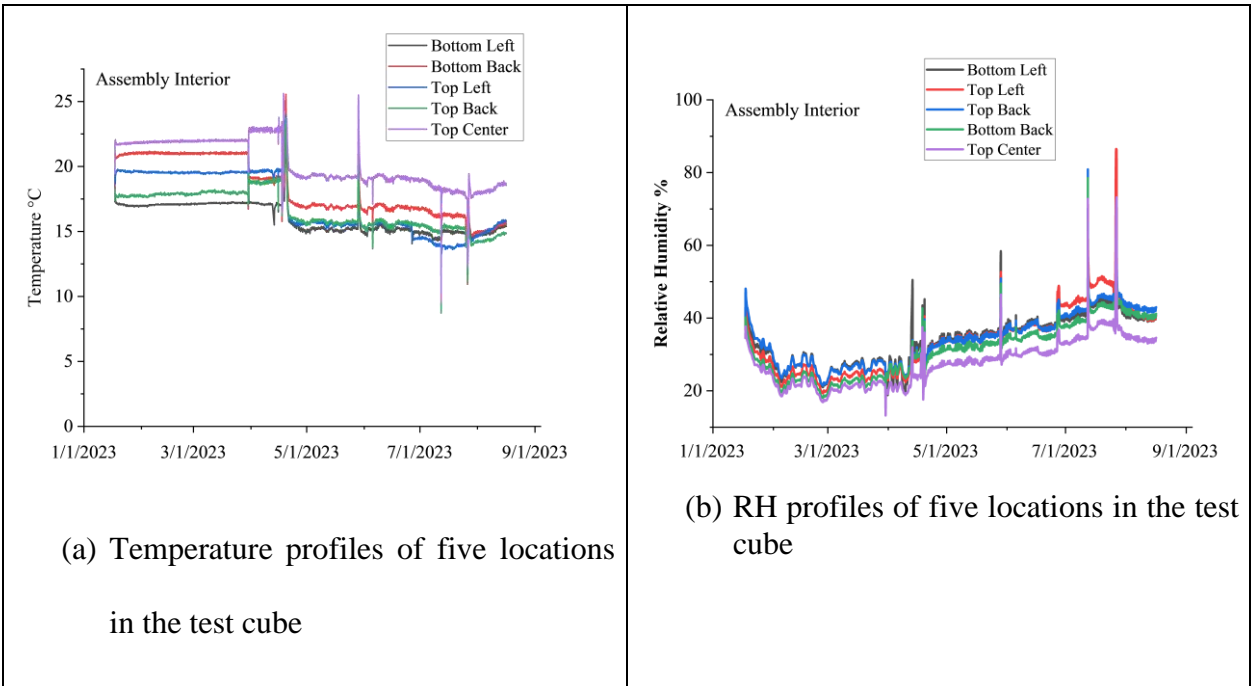
Figure 2. 9: Assembly Interior Conditions
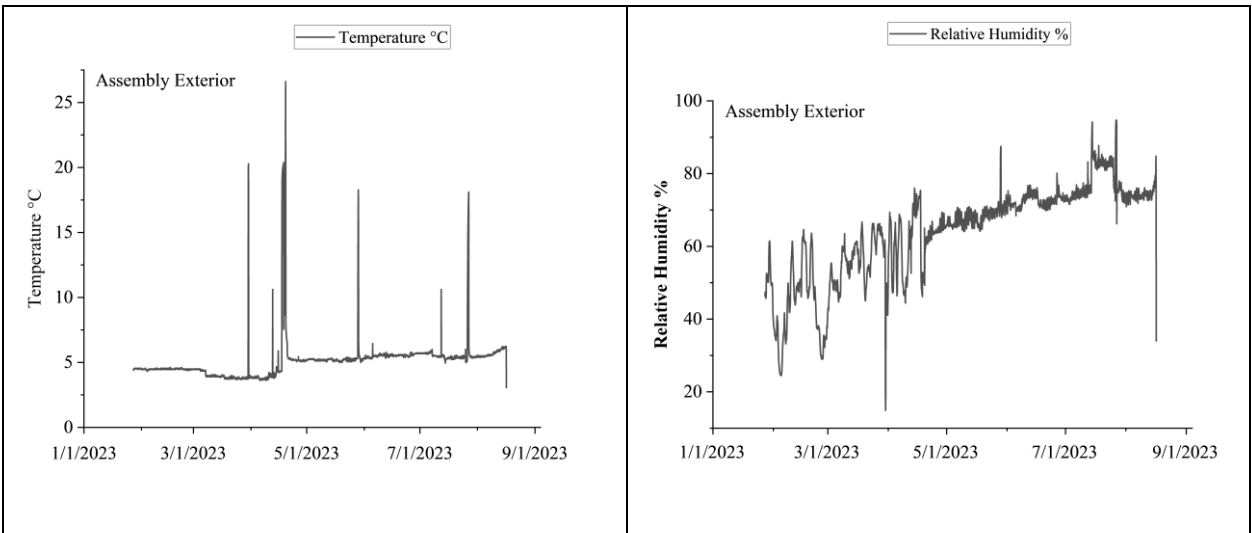
Figure 2. 10: Assembly Exterior Conditions
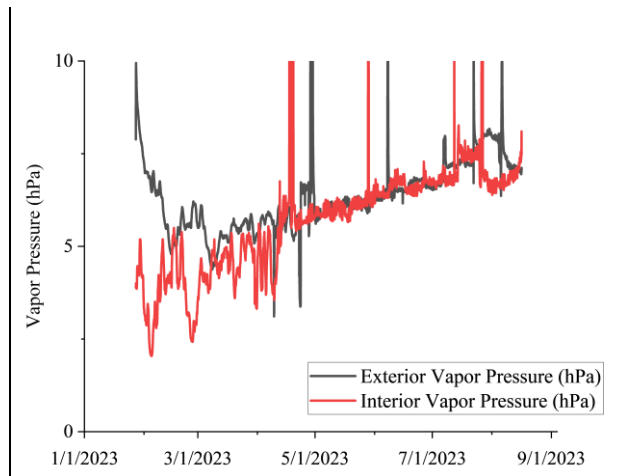
Figure 2. 11: Vapor Pressure Exterior and Interior.

4.2.   Relative Humidity and Temperature of Panels

Relative humidity (RH) and temperature trends for each replicate are plotted below in Figures 8-13. Each interface, i.e., CLT – WFI, WFI – WFI, and WFI – WRB, is shown together in a single figure. RH and temperature reveal predictable steps from one layer to the next: temperature gradually increases in steps from the exterior to the interior, and RH gradually decreases in steps from the exterior to the interior. Two replicates of each assembly type displayed general agreement. The RH levels at each layer of all six panels never exceeded 90%, indicating that there would not have been any condensation development within the wall assemblies at the conditions simulated during this experiment. This is critical; liquid water, though not necessary for mold development and the degradation of wall assemblies, immediately confers much more moisture into the materials than water vapor does.

RH and temperature trends for the two replicates of Assembly A, adhesively bonded WIPs, are shown below in Figures 2.12 and 2.13. The temperature, when compared to exterior conditions, increased by ≈3.5°C after the first layer of insulation and by ≈6.0°C after the second layer at the center of the panel. Temperature measurements separated by only the adhesive layer showed little to no variation at both bond lines. The RH, when compared to the level outside of the test assembly,

decreased by ≈24% directly interior to the OSB, by ≈10% after the first layer of insulation, by ≈13% after the second layer above the adhesive, and by ≈5% under the adhesive layer. These comparisons were made during the steady state measurements in May 2023. For both temperature and RH, the measurements nearer to the interior were less sensitive to sudden changes in exterior conditions. This effect is most clearly seen in the first three months of RH data, where changes in RH were frequent and significant.

The RH measured beneath the WRB for Assembly A was more variable than the RH measured beneath the WRB of the two control Assembly B assemblies despite the two barriers having similar permeabilities. A probable cause for this discrepancy is the presence of the OSB at that layer for the WIP assemblies versus the hygroscopic and permeable WFI present in that layer for control B, illustrating the ability of natural fibers to act as effective buffers to spikes in relative humidity. The adhesive does appear to have some impact on the flow of moisture. It can be seen that the space above the adhesive at the CLT – WFI interface remained at the initial RH for the majority of the experiment, taking about six months to realign with the location interior of the adhesive. The effect is not replicated at the WFI – WFI interface. This discrepancy is likely a factor of the permeability of the CLT and WFI; at the CLT interface, any moisture between the adhesive and the CLT must dry to the interior or through the CLT member, resulting in much slower drying times. These trends in RH and temperature are consistent between panel 1 and panel 2.
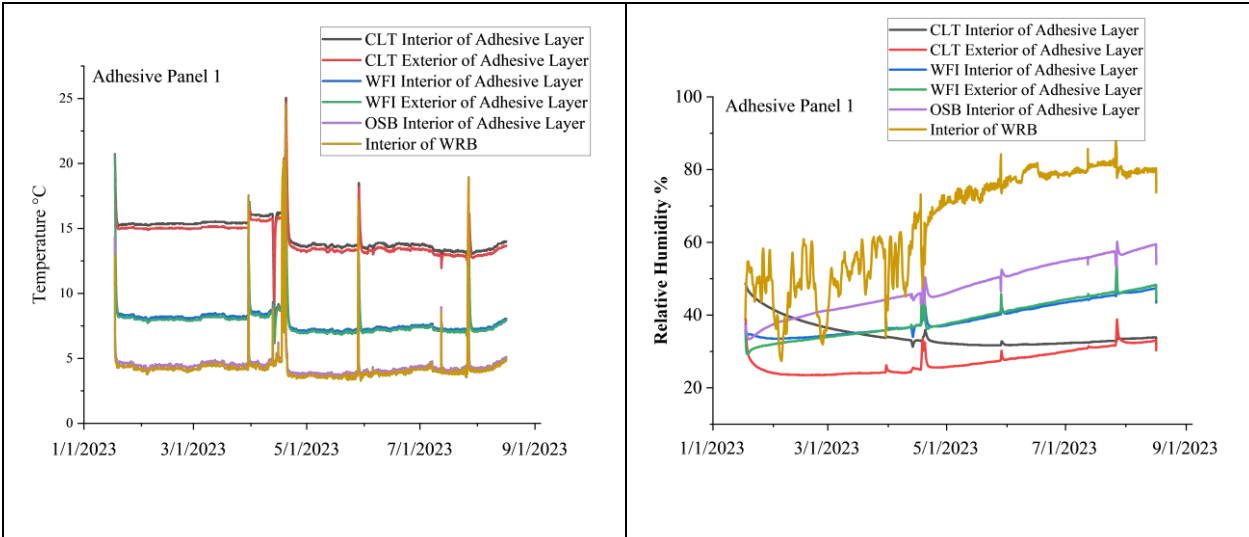
Figure 2. 12: Assembly A: Adhesively Bonded WFI Panel 1
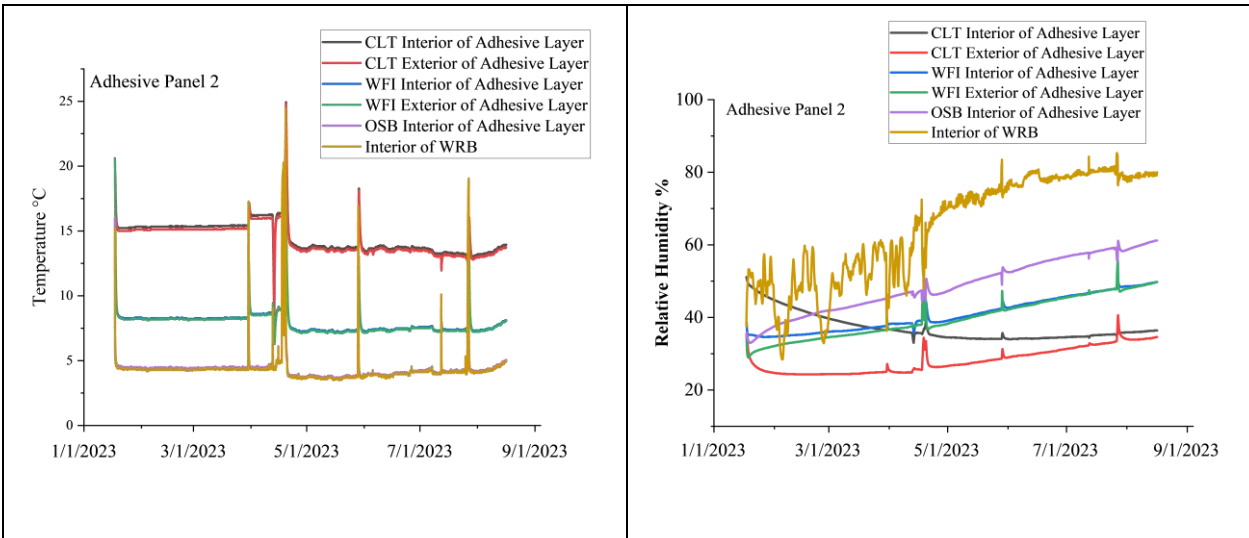
Figure 2. 13. Assembly A: Adhesively Bonded WFI Panel 2

RH and temperature trends for the two replicates of Assembly B, mechanically fastened WFI panels, are shown below in figures 2.14 and 2.15. The temperature increased by ≈3.5°C after the first layer of insulation and by ≈7.5°C after the second layer, at the center of the panel. The temperature increased by ≈2.0°C and ≈5.0°C after each layer of insulation at the site of the lag penetration, indicating thermal loss occurred around the mechanical fastener; a portion of this effect may be influenced by the proximity of the fastener to the edge of the panel. The RH

59

decreased by ≈20% after the first layer of insulation and by ≈15% after the second layer, at the center of the panel. The RH decreases by ≈14% after each layer of insulation at the site of the lag penetration. These comparisons were made using the data collected during May 2023. For both temperature and humidity, the closer to the interior the measurement took place, the less sensitive it was to sudden changes in the exterior conditions. This effect is most clearly seen in the first three months of RH data, where changes in RH were frequent and drastic. These trends in RH and temperature are consistent between panel 1 and panel 2.
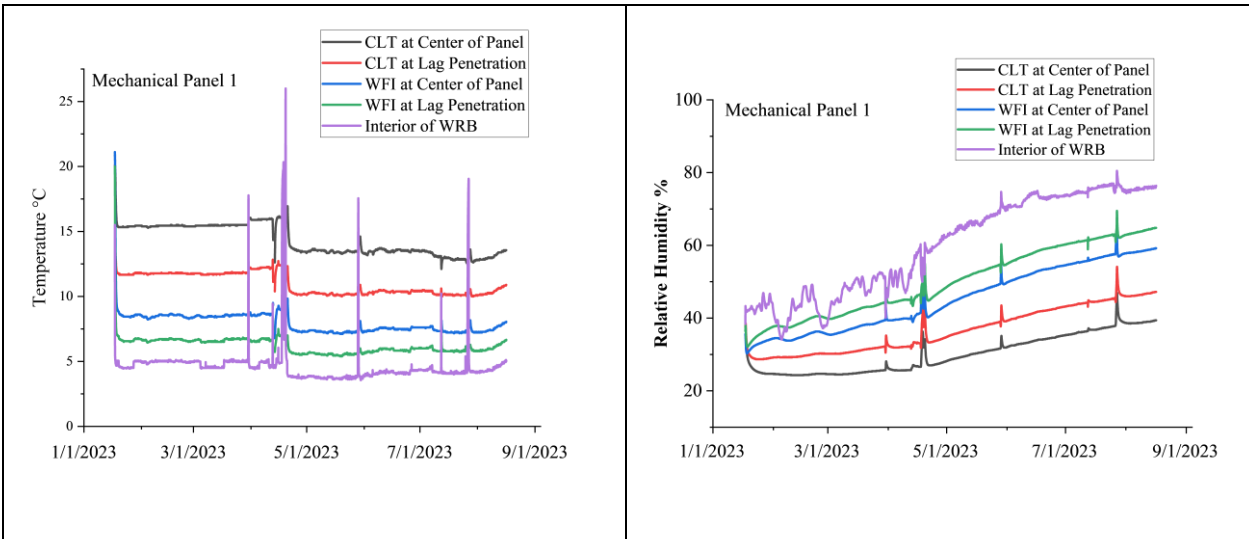
Figure 2. 14: Assembly B: Mechanically Fastened WFI Panel 1
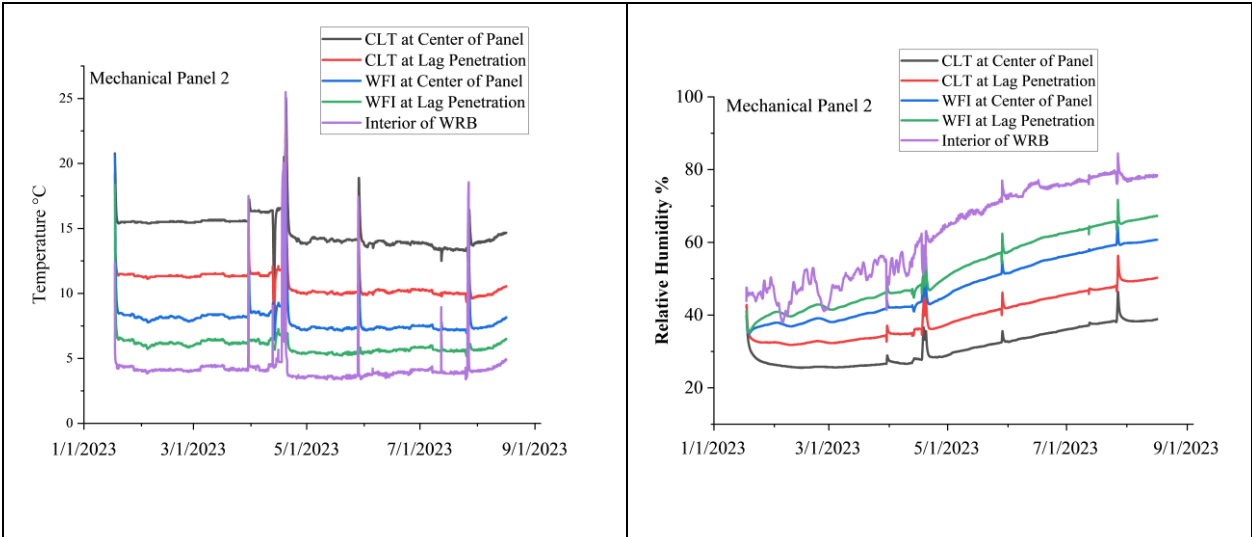
Figure 2. 15. Assembly B: Mechanically Fastened WFI Panel 2

RH and temperature trends for the two replicates of Assembly C, mechanically fastened EPS panels, are shown below in Figures 2.16 and 2.17. The temperature increased by ≈2.5°C after the first layer of insulation and by ≈7.5°C after the second layer at the center of the panel. The temperature increased by ≈1.0°C and ≈6.0°C after each layer of insulation at the site of the lag penetration due to the same reason for thermal loss. The RH began at a much higher level than the chamber's conditions within the EPS layers. This difference between the WFI panels (see Figures 8-11) and the EPS panels (see Figures 12-13) is caused by drying that occurred in the lab during construction and prior to the assembly of the test set-up. The lab conditions were dry, 20% RH, the WFI, and exposed wood materials dried very quickly; the CLT in the EPS panels maintained much of the initial moisture present. Relative humidity at the first insulation interface was ≈50% higher than the chamber conditions at the beginning of the experiment. After two months of steady drying, the RH conditions at the first insulation interface approximated the conditions in the chamber. The monitoring position at the center of the panel and the monitoring position at the lag penetration were broadly similar, with the lag site remaining ≈10% higher throughout the

61

experiment. At the interface between EPS and CLT, the initial conditions were drier than the EPS – EPS interface, ≈80% RH; the RH decreased steadily until May 2023, where it entered into a steady state, ≈55% RH at the center of the panel and ≈60% RH at the lag penetration. The conditions of the interior and exterior of the WRB maintained similar values throughout the experiment. For both temperature and humidity, the closer the measurement took place to the interior, the less sensitive it was to sudden changes in the exterior conditions. This effect is most clearly seen in the first three months of RH data, where changes in RH were frequent and drastic, this can be seen to be even more impactful in the EPS panels than it was in the WFI panels. These trends in RH and temperature are consistent between panel 1 and panel 2.
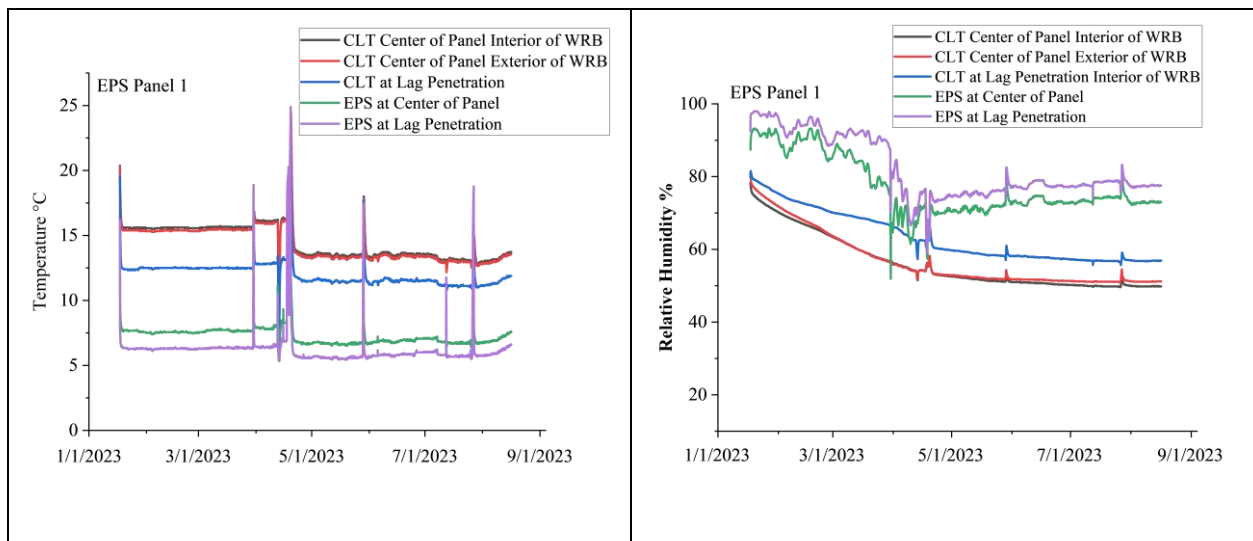
Figure 2. 16: Assembly C: Mechanically Fastened EPS Panel 1
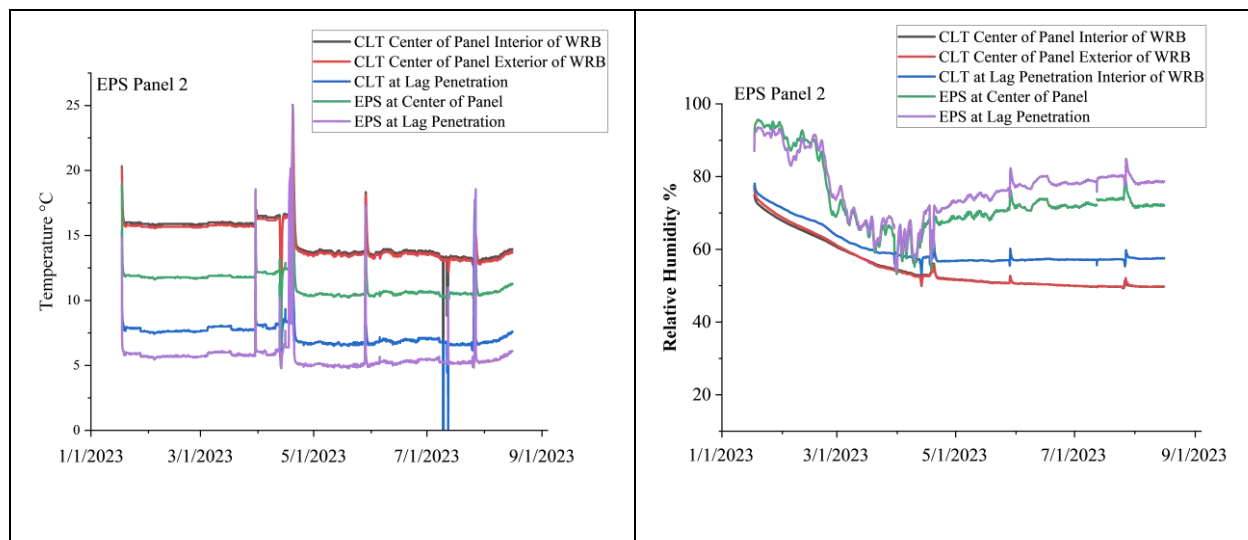
Figure 2. 17: Assembly C: Mechanically Fastened EPS Panel 2

4.3. MC of CLT and OSB

Moisture content data for all six panels are shown below in Figures 2.18 – 2.20. Similar patterns can be observed for all panels. The moisture content of the interior CLT faces dried by ≈2% MC over the course of the eight-month experiment, regardless of the initial MC. In contrast, the differentiation of MC of the CLT layer near the exterior side between three assembly types is more significant, with variations depending on the presence or absence of mechanical fasteners. It is noted that for all assemblies measured, the initial MC of the CLT layer facing the interior of the cube was about 8%, which is lower than that of the CLT layer facing the exterior side by 3 or 4%. The reason might attributable to the assemblies being directly exposed to the ambient environment after assembling. In the dry wintertime, the bare CLT layers began drying before the environmental chamber testing. The other side of the CLT was enclosed in the assembly. A detailed discussion is as follows.

Figure 2.18, below, outlines explicitly the wood moisture content data for Assembly A, the WIP panels. Moisture content was measured at the center of the CLT layer facing the interior of the cube, at the CLT – WFI interface, and at the WFI – OSB interface. The CLT layer facing the

exterior surface and the interior surface had different initial MCs, about 10 or 11% (see red solid lines in Figure 14) and 8% (see black solid lines in Figure 14), respectively, and both dried to 6% MC. However, the OSB had an initial MC at around 6% but began to increase in May 2023 and continued to rise throughout the remainder of the experiment until its end in August at 13% MC.
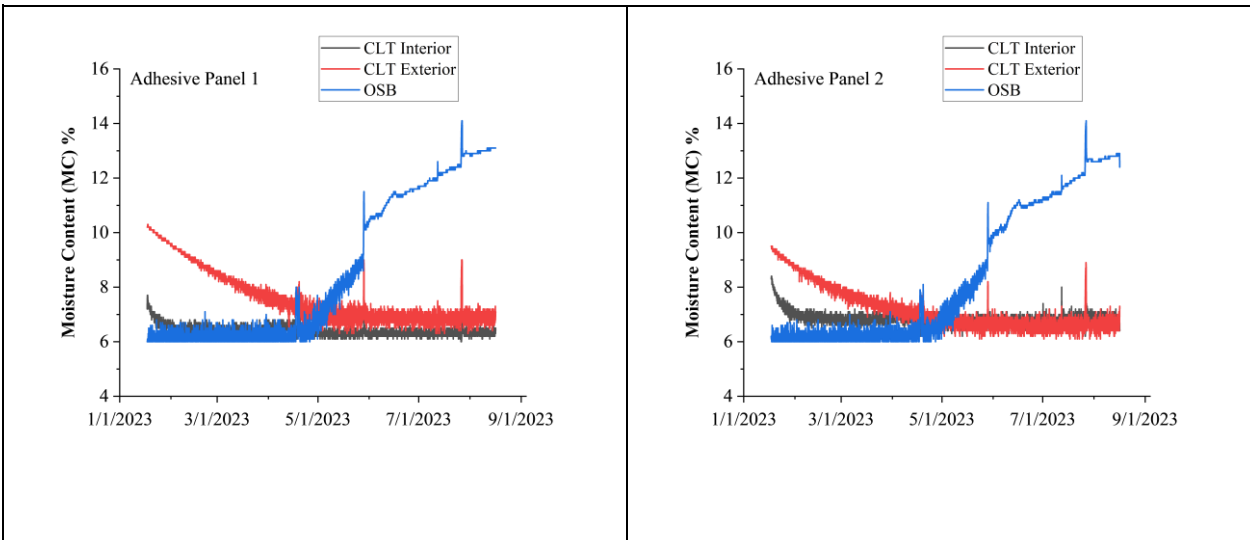
Figure 2. 18: Assembly A: Adhesively Bonded WFI Panels 1 & 2

Moisture content for two replicates of Control Assembly B can be seen below in Figure 2.19. The CLT MC in these assemblies follows the same trend as Assembly A discussed above, with the exception of the exterior surface-reaching equilibrium at ≈7.5% MC, as opposed to 6.0%. The impact of the lag penetration on the moisture content of the CLT can be seen here. The decreased temperature at this point maintained the CLT moisture content at ≈10.0% MC throughout the experiment, as less drying was possible at a lower temperature as compared to the center of the panel area.
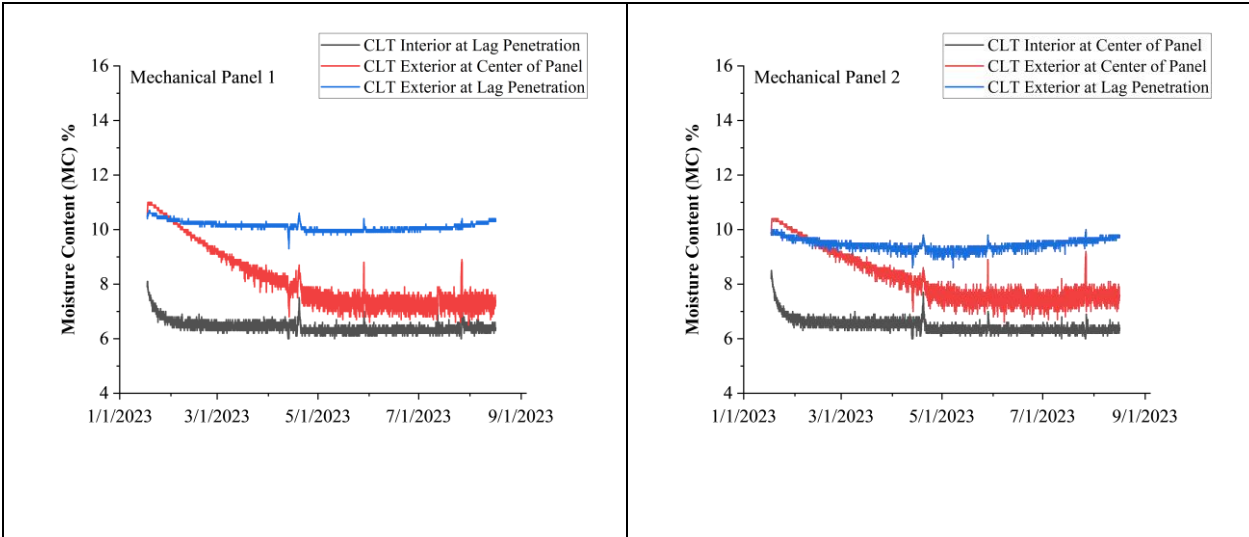
Figure 2. 19: Assembly B: Mechanically Fastened WFI Panels 1 & 2

Moisture content for both replicates of Assembly C can be seen below in Figure 2.20. The interior of the CLT in these assemblies follows the same trend as that of assemblies A and B discussed above. The exterior surface of the CLT maintained a much higher moisture content level throughout the experiment. The wood against the surface of the EPS experiences a significantly decreased the rate of drying when compared to the WFI assemblies; the assemblies approached equilibrium after eight months, while the previously discussed assemblies approached equilibrium after four months. The impact of the lag penetration on the moisture content of the CLT can be seen here as well. The decreased temperature resulted in a CLT moisture content of ≈13.0% MC throughout the experiment, with only a slight decrease over the eight months. The MC data for the CLT exterior of panel 2 was corrupted after three months and did not represent the conditions present in the panel.
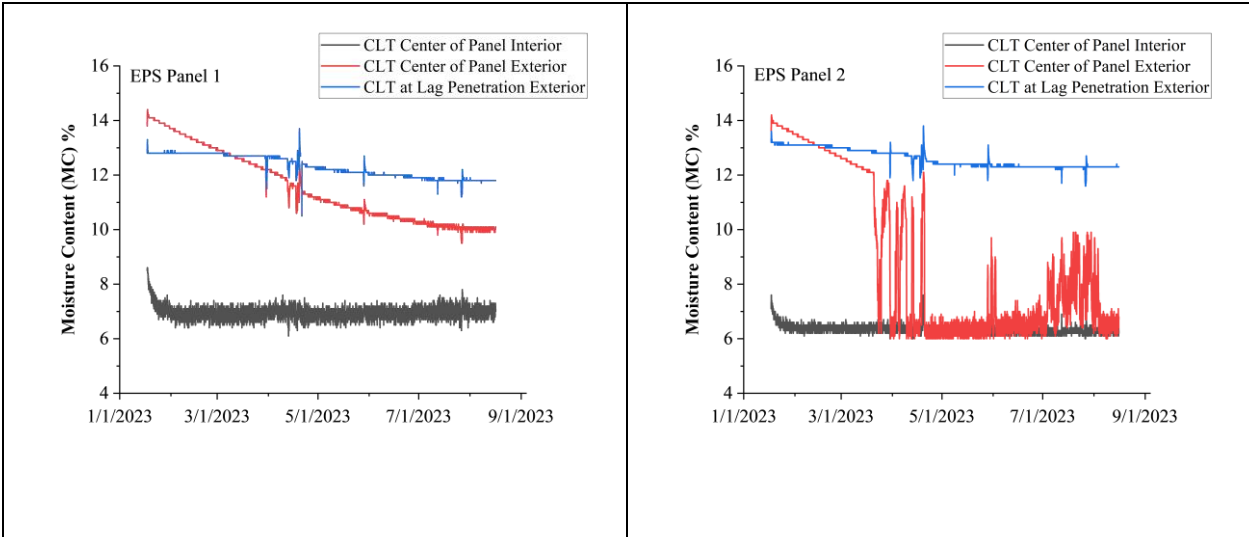
Figure 2. 20: Assembly C: Mechanically Fastened EPS Panels 1 & 2

4.4. Heat Flux, Calculated Total Thermal Conductivity, and Total Thermal Resistance

4.4.1. Experimental Results of Heat Flux and the Resultant Total Thermal Resistance

Tabulated heat flux data for each assembly type can be seen below in Table 2.4. Measurements were made at the center of every assembly and at one lag penetration for each mechanically fastened panel assembly. This made for a total of ten measurement locations: two measurements for Assembly A, four measurements for Assembly B, and four measurements for Assembly C. Each heat flux measurement location had a thermocouple measuring interior and exterior surface temperature. Additionally, the heat flux was measured for all assemblies during a period of steady-state heat flow, not averaged over a period of change.

Assembly A.1 had an average measured heat flux of 2.24 (W/m^2) and a resultant R-value of 5.37 (m^2*K/W). Assembly A.2 had an average heat flux of 2.15 (W/m2) and a resultant R-value of 5.57 (m^2*K/W). The difference between the two heat flux results is within 5%, indicating the variation between the two results is acceptable.

Assembly B.1 had an average measured heat flux of 1.96 (W/m^2) at the center of the panel and an average measured heat flux of 2.76 (W/m^2) at the fastener site. The calculated R-value of B.1 at the center was 6.12 (m^2*K/W) and 4.35 (m^2*K/W) at the fastener site. Assembly B.2 had an average measured heat flux of 1.98 (W/m^2) at the center of the panel and an average measured heat flux of 2.02 (W/m^2) at the fastener site. The measured R-value of B.2 at the center of the panel was 6.05 (m^2*K/W) and 5.94 (m^2*K/W) at the fastener site. The difference between the two heat flux results measured at the center of the panel was within 5%. However, the results measured at each fastener site, panels B.1 and B.2, vary by 36%. The location of this panel may be the cause of this discrepancy from the other mechanically fastened panels. The panel having been located at the bottom of the assembly may have influenced the flow of heat through that panel, resulting in a smaller differential between the two locations. Another possibility is that the sensor did not represent an area affected by the fastener. If the fastener was installed at an angle, then the area of effect could have been different than the other fasteners measured.

Assembly C.1 had an average measured heat flux of 2.20 (W/m^2) at the center of the panel and an average measured heat flux of 2.69 (W/m^2) at the fastener site. The resultant R-value of C.1 at the center of the panel was 5.45 (m^2*K/W) and 4.47 (m^2*K/W) at the fastener site. Assembly C.2 had an average measured heat flux of 2.27 (W/m^2) at the center of the panel and an average measured heat flux of 2.54 (W/m^2) at the fastener site. The difference between the two heat flux measurements made at the center of the panel was within 4%, while that of the two results measured at the fastener site was about 6%. These variances align with those previously observed for Assembly A.1, A.2, and B.1.

The testing results clearly show that these changes in heat flux at the fastener site resulted in a significant increase in heat flux and total thermal conductivity. Using the total R-value as an example, the point thermal bridge caused by the mechanical fastener reduced thermal resistance by an average of 16.56% in Assembly B and by an average of 15.66% in Assembly C. The influence of insulation type on the reduction of total R-value is negligible. Although the cross-sectional area of one screw fastener is limited compared to the overall surface area of the assembly, increasing the number of fasteners per unit area in some applications, such as sloped roof panels, would result in a considerable reduction in the apparent total R-value.

Table 2. 4: Summary of Measured Heat Flux Values.

Panel	Assembly A: 1 &2		Assembly B: 1 & 2				Assembly C: 1 & 2			
Sensor Location	Center- WFI panel		Center - WFI Panel		Lag - WFI panel		Center- EPS Panel		Lag - EPS panel	
Panel Location	Front	Back	Top	Bottom	Top	Bottom	Left	Right	Left	Right
Conversion factor, V/(W/m^2)	6.29E-05	7.00E-05	6.48E-05	6.53E-05	6.81E-05	6.49E-05	6.55E-05	6.99E-05	6.86E-05	6.46E-05
Average Heat Flux, (W/m^2)	2.48	2.41	2.21	2.15	3.11	2.19	2.42	2.45	2.95	2.75
ΔK	13.33	13.41	13.52	13.02	13.52	13.02	13.16	12.97	13.16	12.97
Conductance, (W/m^2*K)	0.19	0.18	0.16	0.17	0.23	0.17	0.18	0.19	0.22	0.21
R-value si, (m^2*K/W)	5.37	5.57	6.12	6.05	4.35	5.94	5.45	5.30	4.47	4.72
Mean R-value si, (m^2*K/W)	5.47		6.08		5.15		5.37		4.59	
Difference[A], %	N/A		16.56				15.66			

A: ((V1-V2)/(V1+V2)/2)) * 100

4.4.2. Theoretical Results of Total Thermal Resistance and Fastener Reduction

Table 2.5 contains the results of calculated R-values for the three assemblies using the equations listed above (Eq. 2.1 - 2.3) from ISO 6946: 2017 *Building components and building elements: thermal resistance and thermal transmittance calculation methods* (ISO, 2017). The thermal resistance for each element of the assembly was calculated based on material values either measured by the author or collected from manufacturers, which are listed in Table 4, and then added together with values provided by the standard for estimating still air and surface resistance to estimate the resistance of the entire assembly.

Table 2. 5: Assembly Layer Thickness and Thermal Resistance.

Material	Resistance of component (m^2*K/W)	Thickness of component (m)	Total Resistance of assembly (m^2*K/W)
CLT	0.890	0.1032	
OSB	0.116	0.0159	
Assembly A: WFI	4.498	0.2159	5.67
Assembly B: WFI	5.027	0.2413	6.06
Assembly C: EPS	4.354	0.1524	5.41

For assemblies B and C, the reduction in overall thermal resistance attributable to the point thermal bridging of fasteners was estimated using the amount of fasteners per square meter, the thermal conductivity of the fastener material, and the cross-sectional area of the fastener shank. The estimated total R-value for each assembly is as follows: Assembly A 5.67 (m^2*K/W), Assembly B 6.06 (m^2*K/W), and Assembly C 5.41 (m^2*K/W). When comparing the measured results in Table 2.4 to the calculated results in Table 2.6, an interesting comparison can be found. The differential

in total R-value between calculated and measured results for each assembly is within 0.20 (m^2*K/W) for Assembly A, 0.02 (m^2*K/W) for Assembly B, and 0.04 (m^2*K/W) for Assembly C. The calculations underestimated the R-value for Assembly B but overestimated for Assemblies A and C. This shows excellent agreement between the measured values and the calculated projections, revealing that the heat flux sensor technique can be applied to in-situ or field measurements of building assembly with unknown material components and geometry information.

Table 2. 6: ISO 6946: 2017 Total R-value and Fastener Reduction.

	Value ID	Value	Value Description and Unit
Assembly A: WIP	d.i	0.22	Depth of insulation layer (m)
	R.i	4.50	Thermal Resistance of insulation layer (m^2*K/W)
	R.tot[a]	5.67	Sum of R for each layer of component (m^2*K/W)
	U-Value	0.18	(W/m^2*K)
	ΔU-Reduction	N/A	(W/m^2*K)
	R-Value Adjst.	N/A	(m^2*K/W)
	Percent Change	N/A	Percent change between adjusted and unadjusted
Assembly B: Mech WFI	α	0.80	0.8 constant from the standard for full fastener penetration
	λ.f	14.40	Thermal conductivity of fastener material (W/m*K)
	n.f	4.00[b]	Number of fasteners per (m^2)
	A.f	2.45E-05	Area of fastener (m^2)
	d.i	0.24	Depth of insulation layer (m)
	R.i	5.03	Thermal Resistance of insulation layer (m^2*K/W)
	R.tot[a]	6.06	Sum of R for each layer of component (m^2*K/W)

	Table 2.6. Continued		
	U-Value Unadjst.	0.17	(W/m^2*K)
	ΔU-Reduction	3.23E-05	(W/m^2*K)
	R-Value Adjst.	5.94	(m^2*K/W)
	Percent Change	1.92%	Percent change between adjusted and unadjusted
Assembly C: EPS	α	0.80	0.8 constant from the standard for full fastener penetration
	$\lambda.f$	14.40	Thermal conductivity of fastener material $(W/m*K)$
	n.f	4.00[b]	Number of fasteners per (m^2)
	A.f	2.75E-05	Area of fastener (m^2)
	d.i	0.15	Depth of insulation layer (m)
	R.i[a]	4.35	Thermal Resistance of insulation layer (m^2*K/W)
	R.tot	5.41	Sum of R for each layer of component (m^2*K/W)
	U-Value Unadjst.	0.18	(W/m^2*K)
	ΔU-Reduction	5.38E-03	(W/m^2*K)
	R-Value Adjst.	5.26	(m^2*K/W)
	Percent Change	2.83%	Percent change between adjusted and unadjusted

[a] Values include still air and surface resistance
[b] Value based on a fastener schedule of 40.64 cm horizontal and 60.96 cm vertical centered in the space

Based on ISO 6946, the total R-value of the assemblies would be reduced by 1.92% in the case of

Assembly B and 2.83% in the case of Assembly C, both reductions are applied to the entire area

of the wall and not a distinct point. The reduction in thermal resistance at the lag site measured by

the heat flux sensors was measured to be significantly greater than that, the sensors showed a local

increase in heat flux of 15-16%. One explanation for this discrepancy is the fact that the ISO

calculations estimate a total reduction over one square meter without considerations for 3-dimensional heat flow and the heat flux measurements are a comparison between two distinct locations. Additionally, the heat flux measurements at the fastener site are not likely to be entirely free from edge effects. The heat flux sensors are reading the area next to the fasteners, not the heat flow through the fastener itself. This means that they are reading the flow of heat that is traveling from the fastener into the surrounding material. There are equations that estimate the 3-dimensional heat flow of fasteners. However, the inputs and time required to implement them are beyond the scope of this study and are outside of the purview of many designers, given the material information that is readily available. The estimation of point thermal bridges can be difficult for many buildings, particularly buildings with high performance, i.e., thick wall assemblies, as these assemblies would not only have larger fasteners more frequently placed throughout the wall but additionally, the increased depth would increase the amount of 3-dimensional heat flow in the assembly, further limiting the applicability of simple thermal bridge calculations. Investigations into the comparability of these different methods will be more and more important as high-performance wall assemblies, R-3.50 and greater, become more commonplace for building codes in mixed climates.

5. CONCLUSION

In this study, the hygrothermal characteristics of adhesively bonded wood fiber insulated panels were thoroughly examined to gain an understanding of how these materials would perform, in a cold climate in comparison to the performance of wood fiber insulated walls with mechanical fasteners and expanded polystyrene insulated walls with mechanical fasteners. This understanding is crucial in determining the viability of these manufacturing techniques while still achieving the

performance required to comply with specific building codes or certifications like PassivHaus while not creating a significant risk of mold growth within the building envelope.

The primary research findings are below:

1) The presence of a hygroscopic and permeable insulation material had a distinct positive impact on the moisture performance of the wall assembly, significantly reducing the level of humidity present in the wall and reducing the impact of climactic spikes in humidity, comparatively to the EPS assemblies. Thermally, the WFI and EPS both performed similarly to their calculated insulative value.

2) It could be seen that the presence or absence of mechanical fasteners had a significant impact on the localized temperature, humidity, and heat flux through the wall assembly; resulting in higher temperatures, higher levels of relative humidity, and higher heat flux values. Reducing or eliminating the presence of mechanical fasteners that penetrate the entire assembly would increase the performance of wood fiber insulated wall assemblies.

3) The adhesive layer in the WIP assemblies did not have any measured detrimental impact on the hygrothermal performance of the wall assemblies. The adhesive being applied as a non-continuous bead allowed moisture to pass through the assembly in much the same manner as without the adhesive. The manufacturing method proposed in this work, the substitution of some or all mechanical fasteners in prefabricated WFI walls, seems to present the opportunity to improve the performance of these walls without introducing any concerns of reduced permeability.

This study was not an exhaustive investigation of this manufacturing technique or its impacts on hygrothermal performance; much work remains to be done. An investigation of different

assemblies using adhesive instead of fasteners would provide valuable information about the feasibility of this method beyond the single assembly investigated here. Characterization of the permeability of these components with and without adhesive or fasteners could provide succinct insight into the impact of using these adhesives. Physical testing investigating the long-term strength, i.e., creep, of these composites would be required prior to their implementation. Calibrated hygrothermal models of different adhesively bonded wall assemblies could be used to investigate different wall designs rapidly.

1. DECLARATION OF COMPETING INTERESTS

The authors declare that they have no known competing financial interests or personal relationships that could have appeared to influence the work reported in this paper.

2. LEGAL DISCLAIMER

This report was prepared as an account of work sponsored by an agency of the United States Government. Neither the United States Government nor any agency thereof, nor any of their employees, makes any warranty, express or implied, or assumes any legal liability or responsibility for the accuracy, completeness, or usefulness of any information, apparatus, product, or process disclosed, or represents that its use would not infringe privately owned rights. Reference herein to any specific commercial product, process, or service by trade name, trademark, manufacturer, or otherwise does not necessarily constitute or imply its endorsement, recommendation, or favoring by the United States Government or any agency thereof. The views and opinions of authors expressed herein do not necessarily state or reflect those of the United States Government or any agency thereof.

BIBLIOGRAPHY

Chapter 1

APA. (2013). ANSI 405-2008: *Standard for Adhesives for Use in Structural Glued Laminated Timbers* (ANSI 405-2008). APA. www.apawood.org

Architecture 2030. (2021). *Why The Built Environment – Architecture 2030*. Www.architecture2030.org. https://www.architecture2030.org/why-the-built-environment/

ASTM International. (2019). ASTM D5751-99 (2019): *Specification for Adhesives Used for Laminate Joints in Nonstructural Lumber Products*. ASTM Compass, 15.06. https://doi.org/10.1520/d5751-99r19

ASTM International. (2020a). *ASTM C209-20: Test Methods for Cellulosic Fiber Insulating Board*. ASTM Compass. https://doi.org/10.1520/c0209-20

ASTM International. (2020b). *ASTM C1763-20: Test Method for Water Absorption by Immersion of Thermal Insulation Materials*. ASTM Compass. https://doi.org/10.1520/c1763-20

ASTM International. (2021a). *ASTM C518 -21: Test Method for Steady-State Thermal Transmission Properties by Means of the Heat Flow Meter Apparatus*. ASTM Compass. https://doi.org/10.1520/c0518-21

ASTM International. (2021b). *ASTM D905-08(2021): Test Method for Strength Properties of Adhesive Bonds in Shear by Compression Loading*. ASTM Compass. https://doi.org/10.1520/d0905-08r21

ASTM International. (2022). ASTM E119-22: *Standard Test Methods for Fire Tests of Building Construction and Materials*. ASTM Compass.

ASTM International. (2023a). ASTM C1058/C1058M − 10: *Practice for Selecting Temperatures for Evaluating and Reporting Thermal Properties of Thermal Insulation*. ASTM Compass. https://doi.org/10.1520/c1058_c1058m-10r23

ASTM International. (2023b). *ASTM E96/E96M-22ae1: Test Methods for Gravimetric Determination of Water Vapor Transmission Rate of Materials*. ASTM Compass. https://doi.org/10.1520/e0096_e0096m-22ae01

Belakroum, R., Gherfi, A., Bouchema, K., Gharbi, A., Kerboua, Y., Kadja, M., Maalouf, C., Mai, T. H., El Wakil, N., & Lachi, M. (2017). Hygric buffer and acoustic absorption of new building insulation materials based on date palm fibers. *Journal of Building Engineering*, *12*, 132–139. https://doi.org/10.1016/j.jobe.2017.05.011

Brambilla, A., & Sangiorgio, A. (2020). Mould growth in energy efficient buildings: Causes, health implications and strategies to mitigate the risk. *Renewable and Sustainable Energy Reviews*, *132*, 110093. https://doi.org/10.1016/j.rser.2020.110093

Cetiner, I., & Shea, A. D. (2018). Wood waste as an alternative thermal insulation for buildings. *Energy and Buildings*, *168*, 374–384. https://doi.org/10.1016/j.enbuild.2018.03.019

Ciancio, V., Falasca, S., Golasi, I., Curci, G., Coppi, M., & Salata, F. (2018). Influence of Input Climatic Data on Simulations of Annual Energy Needs of a Building: EnergyPlus and WRF Modeling for a Case Study in Rome (Italy). *Energies*, *11*(10), 2835. https://doi.org/10.3390/en11102835

De Ligne, L., Van Acker, J., Baetens, J. M., Omar, S., De Baets, B., Thygesen, L. G., Van den Bulcke, J., & Thybring, E. E. (2022). Moisture Dynamics of Wood-Based Panels and Wood Fibre Insulation Materials. *Frontiers in Plant Science*, *13*. https://doi.org/10.3389/fpls.2022.951175

Donato, I. D., & Lazzara, G. (2012). Porosity determination with helium pycnometry as a method to characterize waterlogged woods and the efficacy of the conservation treatments. *Archaeometry*, *54*(5), 906–915. https://doi.org/10.1111/j.1475-4754.2011.00657.x

Euring, M., Kirsch, A. A., & Kharazipour, A. (2015). Hot-Air/Hot-Steam process for the production of laccase-mediator-system bound wood fiber insulation boards. *Bioresources*, *10*(2). https://doi.org/10.15376/biores.10.2.3541-3552

Faghri, A., & Zhang, Y. (2006). *Transport phenomena in multiphase systems with phase change* (pp. 1–106). Academic Press. https://www.sciencedirect.com/science/article/abs/pii/B9780123706102500064

Hameury, S. (2005). Moisture buffering capacity of heavy timber structures directly exposed to an indoor climate: A numerical study. *Building and Environment*, *40*(10), 1400–1412. https://doi.org/10.1016/j.buildenv.2004.10.017

ICC Evaluation Service. (2020). ICC-ES: AC05 - Sandwich Panel Adhesives (AC05 5-2020).

Karagiozis, A., Künzel, H., Holm., A., & WUFI. (2001). WUFI-ORNL/IBP Hygrothermal Model. Buildings VIII/Moisture Model Inputs—Principles.

Kermani, A. (2006). Performance of structural insulated panels. Proceedings of the Institution of Civil Engineers - Structures and Buildings, 159(1), 13–19. https://doi.org/10.1680/stbu.2006.159.1.13

Kirsch, A., Ostendorf, K., & Euring, M. (2018). Improvements in the production of wood fiber insulation boards using hot-air/hot-steam process. *European Journal of Wood and Wood Products*, *76*(4), 1233–1240. https://doi.org/10.1007/s00107-018-1306-z

Koizumi, Y., Shoji, M., Monde, M., Takata, Y., & Nagai, N. (2017). *Boiling* (pp. 443–777). Elsevier. https://www.sciencedirect.com/science/article/pii/B9780081010105000063

Kunič, R. (2017). Carbon footprint of thermal insulation materials in building envelopes. *Energy Efficiency*, *10*(6), 1511–1528. https://doi.org/10.1007/s12053-017-9536-1

Lawrence, M., Shea, A., Walker, P., & De Wilde, P. (2013). Hygrothermal performance of bio-based insulation materials. *Proceedings of the Institution of Civil Engineers - Construction Materials*, *166*(4), 257–263. https://doi.org/10.1680/coma.12.00031

Meissner, J. W., Mendes, N., Mendonça, K. C., & Moura, L. M. (2010). A full-scale experimental set-up for evaluating the moisture buffer effects of porous material. *International Communications in Heat and Mass Transfer*, *37*(9), 1197–1202. https://doi.org/10.1016/j.icheatmasstransfer.2010.07.022

Muthuraj, R., Lacoste, C., Lacroix, P., & Bergeret, A. (2019). Sustainable thermal insulation biocomposites from rice husk, wheat husk, wood fibers and textile waste fibers: Elaboration and performances evaluation. Industrial Crops and Products, 135, 238–245. https://doi.org/10.1016/j.indcrop.2019.04.053

O'Dwyer, J., Walshe, D., & Byrne, K. A. (2018). Wood waste decomposition in landfills: An assessment of current knowledge and implications for emissions reporting. *Waste Management*, *73*, 181–188. https://doi.org/10.1016/j.wasman.2017.12.002

Osanyintola, O. F., & Simonson, C. J. (2006). Moisture buffering capacity of hygroscopic building materials: Experimental facilities and energy impact. *Energy and Buildings*, *38*(10), 1270–1282. https://doi.org/10.1016/j.enbuild.2006.03.026

Pacheco-Torgal, F., Jalali, S., & Fucic, A. (2012). *Toxicity of building materials*. Woodhead Publishing.

Palumbo, M., Lacasta, A. M., Holcroft, N., Shea, A., & Walker, P. (2016). Determination of hygrothermal parameters of experimental and commercial bio-based insulation materials. *Construction and Building Materials*, *124*, 269–275. https://doi.org/10.1016/j.conbuildmat.2016.07.106

Rose, W. B. (1992). Measured Values of Temperature and Sheathing Moisture Content in Residential Attic Assemblies. *Proceedings of the ASHRAE/DOE/BTECC Conference*. December 7-10, Clearwater Beach, Florida. American Society of Heating Refrigeration and Air-Conditioning Engineers, Atlanta.

Salonvaara, M. (2004). Moisture buffering effects on indoor air quality-experimental and simulation results. *Proceedings (CD) of the Performance of Exterior Envelopes of Whole Buildings IX International Conference.*. Vol. 11. Florida: Clearwater Beach, 2004.

Schiavoni, S., D'AlessandroF., Bianchi, F., & Asdrubali, F. (2016). Insulation materials for the building sector: A review and comparative analysis. *Renewable and Sustainable Energy Reviews*, *62*(62), 988–1011. https://doi.org/10.1016/j.rser.2016.05.045

Simonson, C. J., Salonvaara, M., & Ojanen, T. (2004a). Heat and Mass Transfer between Indoor Air and a Permeable and Hygroscopic Building Envelope: Part I – Field Measurements. *Journal of Thermal Envelope and Building Science*, *28*(1), 63–101. https://doi.org/10.1177/1097196304044395

Simonson, C. J., Salonvaara, M., & Ojanen, T. (2004b). *Moderating indoor conditions with hygroscopic building materials and outdoor ventilation*. 804–819. ASHRAE Transactions 110.2 .

Stec, A. A., & Hull, T. R. (2011). Assessment of the fire toxicity of building insulation materials. *Energy and Buildings*, *43*(2-3), 498–506. https://doi.org/10.1016/j.enbuild.2010.10.015

Stock, G. (2021, May 2). *Why NETZSCH Heat Flow Meters Support Reduction of C02 Emissions*. Netzsch.com. https://analyzing-testing.netzsch.com/en/blog/2021/why-netzsch-heat-flow-meters-support-reduction-of-c02-emissions

Veitmans, K., & Grinfelds, U. (2016). Wood fiber insulation material. *Research for Rural Development*, *Vol. 2*(ISSN 2255-923X), 91–98.

Vololonirina, O., Coutand, M., & Perrin, B. (2014). Characterization of hygrothermal properties of wood-based products – Impact of moisture content and temperature. *Construction and Building Materials*, *63*, 223–233. https://doi.org/10.1016/j.conbuildmat.2014.04.014

Winandy, J. E., & Hatfield, C. A. (2007). Analysis of three-year Wisconsin temperature histories for roof systems using wood, wood-thermoplastic composite, and fiberglass shingles. *Forest Products Journal*, *57*(9), 87–96.

Zhuang, B., Cloutier, A., & Koubaa, A. (2022). Physical and Mechanical Properties of Oriented Strand Board Made from Eastern Canadian Softwood Species. *Forests*, 13(4), 523. https://doi.org/10.3390/f13040523

Chapter 2

Arehart, J. H., Hart, J., Pomponi, F., & D'Amico, B. (2021). Carbon sequestration and storage in the built environment. *Sustainable Production and Consumption*, *27*, 1047–1063. https://doi.org/10.1016/j.spc.2021.02.028

ASTM International. (2020). Test Methods for Direct Moisture Content Measurement of Wood and Wood-Based Materials. *ASTM Compass*. https://doi.org/10.1520/d4442-20

ASTM International. (2021). *ASTM C1046-95: Practice for In-Situ Measurement of Heat Flux and Temperature on Building Envelope Components*. ASTM Compass. https://doi.org/10.1520/c1046-95r21

Berardi, U., & Ákos, L. (2019). Thermal bridges of metal fasteners for aerogel-enhanced blankets. *Energy and Buildings*, *185*, 307–315. https://doi.org/10.1016/j.enbuild.2018.12.041

Depro, B. M., Murray, B. C., Alig, R. J., & Shanks, A. (2008). Public land, timber harvests, and climate mitigation: Quantifying carbon sequestration potential on U.S. public timberlands. *Forest Ecology and Management*, *255*(3-4), 1122–1134. https://doi.org/10.1016/j.foreco.2007.10.036

Environmental Protection Agency Clean Air Act Advisory Committee. (2006). Recommendations for reducing emissions from the Legacy Diesel Fleet. US Environmental Protection Agency, Washington DC.

Emmerich, S. J., McDowell, T. P., & Anis, W. (2007). Simulation of the Impact of Commercial Building Envelope Airtightness on Building Energy Utilization | NIST. *ASHRAE Transactions*, *113*.

Fan, Y., Kameishi, K., Onishi, S., & Ito, K. (2014). Field-based study on the energy-saving effects of CO_2 demand controlled ventilation in an office with application of Energy recovery ventilators. *Energy and Buildings*, *68*, 412–422. https://doi.org/10.1016/j.enbuild.2013.09.043

Forest Products Laboratory. 2021. Wood handbook—wood as an engineering material. General Technical Report FPL-GTR-282. Madison, WI: U.S. Department of Agriculture, Forest Service, Forest Products Laboratory. 543 p

FPInnovations. (2013). *CLT : Handbook cross-laminated timber* (E. Karacabeyli & B. Douglas, Eds.). Fpinnovations.

Ge, H., & Baba, F. (2017). Effect of dynamic modeling of thermal bridges on the energy performance of residential buildings with high thermal mass for cold climates. *Sustainable Cities and Society*, *34*, 250–263. https://doi.org/10.1016/j.scs.2017.06.016

Guggemos, A. A., & Horvath, A. (2006). Decision-Support Tool for Assessing the Environmental Effects of Constructing Commercial Buildings. *Journal of Architectural Engineering*, *12*(4), 187–195. https://doi.org/10.1061/(asce)1076-0431(2006)12:4(187)

Hust, J. G., & Lankford, A. B. (1984). Update of thermal conductivity and electrical resistivity of electrolytic iron, tungsten, and stainless steel. *National Bureau of Standards Special Publication*, *260*, 71.

ILOMETS, S., KUUSK, K., PAAP, L., ARUMÄGI, E., & KALAMEES, T. (2016). IMPACT OF LINEAR THERMAL BRIDGES ON THERMAL TRANSMITTANCE OF RENOVATED APARTMENT BUILDINGS. *JOURNAL of CIVIL ENGINEERING and MANAGEMENT*, *23*(1), 96–104. https://doi.org/10.3846/13923730.2014.976259

ISO, E. (2017). 6946: 2017 Building components and building elements—Thermal resistance and thermal transmittance—Calculation methods. *European Committee for Standardization: Brussels, Belgium*.

Khavari, A. M., Pei, S., & Tabares-Velasco, P. C. (2016). Energy Consumption Analysis of Multistory Cross-Laminated Timber Residential Buildings: A Comparative Study. *Journal of Architectural Engineering*, *22*(2), 04016002. https://doi.org/10.1061/(asce)ae.1943-5568.0000206

Kočí, V., Jerman, M., Pavlík, Z., Maděra, J., Žák, J., & Černý, R. (2020). Interior thermal insulation systems based on wood fiberboards: experimental analysis and computational

assessment of hygrothermal and energy performance in the Central European climate. *Energy and Buildings*, *222*, 110093. https://doi.org/10.1016/j.enbuild.2020.110093

Kreiger, B. K., & Srubar, W. V. (2019). Moisture buffering in buildings: A review of experimental and numerical methods. *Energy and Buildings*, *202*, 109394. https://doi.org/10.1016/j.enbuild.2019.109394

Kuittinen, M., Zernicke, C., Slabik, S., & Hafner, A. (2021). How can carbon be stored in the built environment? A review of potential options. *Architectural Science Review*, *66*, 1–17. https://doi.org/10.1080/00038628.2021.1896471

Lantonio, N. A., & Krarti, M. (2022). Simultaneous design and control optimization of smart glazed windows. *Applied Energy*, *328*, 120239. https://doi.org/10.1016/j.apenergy.2022.120239

Levy, J. I., Woo, M. K., Penn, S. L., Omary, M., Tambouret, Y., Kim, C. S., & Arunachalam, S. (2016). *Carbon reductions and health co-benefits from US residential energy efficiency measures*. Environmental Research Letters, 11(3), 034017. https://doi.org/10.1088/1748-9326/11/3/034017

Mao, C., Shen, Q., Shen, L., & Tang, L. (2013). Comparative study of greenhouse gas emissions between off-site prefabrication and conventional construction methods: Two case studies of residential projects. *Energy and Buildings*, *66*, 165–176. https://doi.org/10.1016/j.enbuild.2013.07.033

Mattila, T., Grönroos, J., Judl, J., & Korhonen, M.-R. (2012). Is biochar or straw-bale construction a better carbon storage from a life cycle perspective? *Process Safety and Environmental Protection*, *90*(6), 452–458. https://doi.org/10.1016/j.psep.2012.10.006

Newell, T., & Newell, B. (2011). Thermal mass design. *ASHRAE Journal*, *53*(3), 70-76.

Parameshwaran, R., Kalaiselvam, S., Harikrishnan, S., & Elayaperumal, A. (2012). Sustainable thermal energy storage technologies for buildings: A review. *Renewable and Sustainable Energy Reviews*, *16*(5), 2394–2433. https://doi.org/10.1016/j.rser.2012.01.058

Reba. (2022, July 12). *TSW R&D Study: Embodied Carbon Content of Common Building Materials*. TSW. https://www.tsw-design.com/tsw-rd-study-embodied-carbon-content-of-common-building-materials/

Röck, M., Saade, M. R. M., Balouktsi, M., Rasmussen, F. N., Birgisdottir, H., Frischknecht, R., Habert, G., Lützkendorf, T., & Passer, A. (2020). Embodied GHG emissions of buildings – The hidden challenge for effective climate change mitigation. *Applied Energy*, *258*, 114107. Sciencedirect. https://doi.org/10.1016/j.apenergy.2019.114107

Rüdisser, D. (2018, April). *A brief guide and free tool for the calculation of the thermal mass of building components (according to ISO 13786)*. ResearchGate. http://dx.doi.org/10.13140/RG.2.2.18312.72967/1

Sadauskiene, J., Ramanauskas, J., & Vasylius, A. (2020). Impact of point thermal bridges on thermal properties of building envelopes. *Thermal Science*, *24*(3 Part B), 2181–2188. https://doi.org/10.2298/tsci180719299s

Salonvaara, M., Iffa, E., Desjarlais, A. O., & Atchley, J. (2022). Impact of Mass Wood Walls on Building Energy Use, Peak Demand, and Thermal Comfort. *OSTI OAI (U.S. Department of Energy Office of Scientific and Technical Information)*. https://doi.org/10.2172/1883909

Shafigh, P., Asadi, I., & Mahyuddin, N. B. (2018). Concrete as a thermal mass material for building applications - A review. *Journal of Building Engineering*, *19*, 14–25. https://doi.org/10.1016/j.jobe.2018.04.021

Snow, J., Herzog, B., O'Brien, L., Li, L. (2024). *Characterization of Wood Fiber Insulation for the Development of Wood Fiber-Insulated Panels (WIPs) for Use in Building Envelope. Bioresources.*

Steico. (n.d.). *Steico special dry: Technical Specifications*. STEICO. https://www.steico.com/en/products/insulation/insulation-systems-for-roofs/sarking-and-sheathing-boards/steicospecial-dry

Tang, P., Cass, D., & Mukherjee, A. (2013). Investigating the effect of construction management strategies on project greenhouse gas emissions using interactive simulation. *Journal of Cleaner Production*, *54*, 78–88. https://doi.org/10.1016/j.jclepro.2013.03.046

Theodosiou, T. G., Tsikaloudaki, A. G., Kontoleon, K. J., & Bikas, D. K. (2015). Thermal bridging analysis on cladding systems for building facades. *Energy and Buildings*, *109*, 377–384. https://doi.org/10.1016/j.enbuild.2015.10.037

Toochi, E. C. (2018). Carbon sequestration: how much can forestry sequester CO2? Forestry Research and Engineering: International Journal, 2(3). https://doi.org/10.15406/freij.2018.02.00040

Zhang, M., Qin, M., Rode, C., & Chen, Z. (2017). Moisture buffering phenomenon and its impact on building energy consumption. *Applied Thermal Engineering*, *124*, 337–345. https://doi.org/10.1016/j.applthermaleng.2017.05.173

Appendix A. Compiled Results

Table A.1. Tensile Strength Results

Adhesive	WFI : WFI		WFI : OSB		WFI : SPF	
	Max Load (kg)	Max Stress (kPa)	Max Load (kg)	Max Stress (kPa)	Max Load (kg)	Max Stress (kPa)
PUR-R A-1-1	3.45	12.96	3.10	11.69	3.22	11.92
PUR-R A-1-2	2.54	9.38	3.46	13.17	3.10	11.70
PUR-R A-1-3	2.70	9.98	3.60	13.77	3.23	11.94
PUR-R A-1-4	3.71	13.84	3.56	13.47	3.63	13.26
PUR-R B-1-1	3.07	11.53			3.63	14.13
PUR-R B-1-2	3.10	11.67	3.51	13.50	3.52	13.53
PUR-R B-1-3	2.28	8.46	3.62	14.01	3.92	14.56
PUR-R B-1-4	2.97	11.10	4.14	14.95	4.14	15.33
Mean	**2.98**	**11.12**	**3.57**	**13.51**	**3.55**	**13.30**
Stdev	0.47	1.80	0.31	0.98	0.36	1.35
COV %	15.81%	16.21%	8.59%	7.28%	10.17%	10.16%
Minimum	2.28	8.46	3.10	11.69	3.10	11.70
Maximum	3.71	13.84	4.14	14.95	4.14	15.33

Continued	WFI : WFI		WFI : OSB		WFI : SPF	
Adhesive	**Max Load (kg)**	**Max Stress (kPa)**	**Max Load (kg)**	**Max Stress (kPa)**	**Max Load (kg)**	**Max Stress (kPa)**
PUR-S A-1-1	3.90	14.33	3.96	14.81	3.84	14.07
PUR-S A-1-2	4.15	15.30	4.11	15.41	3.06	11.22
PUR-S A-1-3	2.43	9.10	3.78	14.03	3.72	13.68
PUR-S A-1-4	3.83	14.10	3.97	14.78	3.78	13.88
PUR-S B-1-1	4.08	15.18	3.73	14.04	3.45	12.64
PUR-S B-1-2	4.25	15.75	4.22	15.95	4.04	15.04
PUR-S B-1-3	4.28	15.92	4.67	17.15	3.90	14.43
PUR-S B-1-4	3.32	12.47	3.95	14.59	3.87	14.53
Mean	**3.78**	**14.02**	**4.05**	**15.09**	**3.71**	**13.69**
Stdev	0.63	2.28	0.30	1.05	0.31	1.22
COV %	16.56%	16.25%	7.32%	6.96%	8.39%	8.92%
Minimum	2.43	9.10	3.73	14.03	3.06	11.22
Maximum	4.28	15.92	4.67	17.15	4.04	15.04

Continued	WFI : WFI		WFI : OSB		WFI : SPF	
Adhesive	**Max Load (kg)**	**Max Stress (kPa)**	**Max Load (kg)**	**Max Stress (kPa)**	**Max Load (kg)**	**Max Stress (kPa)**
EPI A-1-1	3.40	12.78	3.23	11.70	3.22	11.89
EPI A-1-2	3.61	13.62	3.41	12.50	4.40	16.19
EPI A-1-3	3.34	12.47	3.41	12.62	4.32	15.93
EPI A-1-4	2.98	11.02	3.50	12.99	3.51	12.80
EPI B-1-1	3.59	13.23	3.30	12.34	4.26	15.60
EPI B-1-2	3.63	13.38	3.37	12.45	4.04	14.75
EPI B-1-3	3.64	13.53	3.19	11.73	3.47	12.96
EPI B-1-4	2.99	11.06	3.05	11.19	4.05	14.94
Mean	**3.40**	**12.63**	**3.31**	**12.19**	**3.91**	**14.38**
Stdev	0.28	1.06	0.14	0.59	0.45	1.62
COV %	8.17%	8.36%	4.37%	4.88%	11.42%	11.26%
Minimum	2.98	11.02	3.05	11.19	3.22	11.89
Maximum	3.64	13.62	3.50	12.99	4.40	16.19

Table A.2. Shear Strength Results

Adhesive	WFI : WFI		WFI : OSB		WFI : SPF	
	Max Load (kg)	Max Stress (kPa)	Max Load (kg)	Max Stress (kPa)	Max Load (kg)	Max Stress (kPa)
PUR-R A-2-1	13.83	77.43	11.52	64.60	10.80	56.98
PUR-R A-2-2	13.65	74.63	14.24	73.41	14.42	76.88
PUR-R A-2-3	11.97	66.58	13.65	73.23	0.00	0.00
PUR-R A-2-4	11.66	67.45	12.02	64.54	15.88	77.72
PUR-R B-2-1	10.84	65.52	10.98	58.59	15.60	83.60
PUR-R B-2-2	12.20	69.49	11.34	64.80	11.39	59.45
PUR-R B-2-3	12.02	68.18	12.02	65.87	21.14	112.62
PUR-R B-2-4	10.30	60.69	11.39	60.17	12.34	65.19
Mean	12.06	68.74	12.14	65.65	12.69	66.55
Stdev	1.22	5.24	1.18	5.35	6.09	32.11
COV %	10.14%	7.63%	9.69%	8.16%	47.96%	48.25%
Minimum	10.30	60.69	10.98	58.59	0.00	0.00
Maximum	13.83	77.43	14.24	73.41	21.14	112.62

Continued	WFI : WFI		WFI : OSB		WFI : SPF	
Adhesive	**Max Load (kg)**	**Max Stress (kPa)**	**Max Load (kg)**	**Max Stress (kPa)**	**Max Load (kg)**	**Max Stress (kPa)**
PUR-S A-2-1	13.65	82.78	15.74	84.09	13.47	73.66
PUR-S A-2-2	13.88	82.54	12.20	65.91	14.47	77.17
PUR-S A-2-3	13.06	71.17	13.38	71.22	11.61	60.68
PUR-S A-2-4	12.52	72.27	17.64	93.26	11.52	60.45
PUR-S B-2-1	14.38	89.14	13.43	72.19	16.69	84.86
PUR-S B-2-2	13.56	83.09	12.11	64.87	12.70	63.97
PUR-S B-2-3	13.43	79.38	12.84	68.37	14.06	74.11
PUR-S B-2-4	14.83	80.69	15.47	82.79	16.19	84.41
Mean	13.66	80.13	14.10	75.34	13.84	72.41
Stdev	0.72	5.92	1.97	10.19	1.92	9.84
COV %	5.29%	7.39%	13.99%	13.53%	13.90%	13.59%
Minimum	12.52	71.17	12.11	64.87	11.52	60.45
Maximum	14.83	89.14	17.64	93.26	16.69	84.86

Continued	WFI : WFI		WFI : OSB		WFI : SPF	
Adhesive	**Max Load (kg)**	**Max Stress (kPa)**	**Max Load (kg)**	**Max Stress (kPa)**	**Max Load (kg)**	**Max Stress (kPa)**
EPI-35 A-2-1	12.52	71.32	11.43	60.36	12.52	65.86
EPI-35 A-2-2	13.34	74.93	14.51	76.05	12.66	66.96
EPI-35 A-2-3	12.16	69.01	18.14	95.33	11.97	64.82
EPI-35 A-2-4	11.88	65.91	11.57	61.16	12.47	67.85
EPI-35 B-2-1	13.88	77.66	12.56	64.19	13.56	69.41
EPI-35 B-2-2	12.38	69.28	11.43	60.08	13.47	69.01
EPI-35 B-2-3	11.97	67.91	11.70	65.71	13.02	68.12
EPI-35 B-2-4	13.70	79.53	12.11	68.31	12.61	67.60
Mean	12.73	71.94	12.93	68.90	12.79	67.45
Stdev	0.79	4.90	2.34	11.91	0.53	1.54
COV %	6.23%	6.81%	18.10%	17.29%	4.18%	2.28%
Minimum	11.88	65.91	11.43	60.08	11.97	64.82
Maximum	13.88	79.53	18.14	95.33	13.56	69.41

Table A.3. Permeance and Permeability Results

| Sample | **Unadjusted** | | | | |
	Slope (g/h)	WVTR (g/h*m^2)	WVP (g/h*m^2*Pa)	WVP (ng/s*m^2*Pa)	Permeability (ng/s*m*Pa)
110W A	0.123	8.61	0.0069	1921.99	76.37
110W B	0.125	8.75	0.0070	1952.72	77.54
110W C	0.125	8.81	0.0071	1966.56	78.21
Mean	0.12	8.72	0.01	1947.09	77.37
Std.Dev	0.00	0.10	0.00	22.82	0.93
COV %	0.79%	1.17%	1.17%	1.17%	1.20%
140W A	0.081	5.752	0.0046	1283.86	78.12
140W B	0.083	5.821	0.0047	1299.38	78.71
140W C	0.079	5.635	0.0045	1257.80	77.32
Mean	0.08	5.74	0.00	1280.35	78.05
Std.Dev	0.00	0.09	0.00	21.01	0.70
COV %	2.32%	1.64%	1.64%	1.64%	0.89%
180W A	0.091	6.49	0.0052	1448.18	57.54
180W B	0.087	6.13	0.0049	1367.84	54.32
180W C	0.095	6.78	0.0054	1513.75	60.19
Mean	0.09	6.47	0.01	1443.26	57.35
Std.Dev	0.00	0.33	0.00	73.08	2.95
COV %	4.34%	5.06%	5.06%	5.06%	5.14%

Continued					
140NW A	0.088	6.15	0.0049	1373.78	81.94
140NW B	0.085	6.05	0.0049	1351.12	81.39
140NW C	0.086	6.06	0.0049	1352.78	81.69
Mean	0.09	6.09	0.00	1359.23	81.68
Std.Dev	0.00	0.06	0.00	12.63	0.27
COV %	1.42%	0.93%	0.93%	0.93%	0.34%
EPS A	0.008	0.586	0.0005	130.82	6.45
EPS B	0.009	0.597	0.0005	133.28	6.56
EPS C	0.010	0.727	0.0006	162.19	7.98
Mean	0.01	0.64	0.00	142.09	6.99
Std.Dev	0.00	0.08	0.00	17.45	0.85
COV %	12.0%	12.28%	12.28%	12.28%	12.17%

Continued	**Adjusted for still air and surface resistance**			
Sample	WVP (ng/s*m^2*Pa)	Permeability (ng/s*m*Pa)	Perms (grains/h*ft^2*inHg)	Permeability (grains/h*ft*inHg)
110W A	2332.33	92.68	40.8	5.32
110W B	2377.75	94.42	41.6	5.42
110W C	2398.30	95.37	42.0	5.48
Mean	2369.46	94.16	41.47	5.41
Std.Dev	33.76	1.37	0.59	0.08

Continued				
COV %	1.42%	1.45%	1.42%	1.45%
140W A	1454.83	88.52	25.5	5.08
140W B	1474.80	89.34	25.8	5.12
140W C	1421.47	87.38	24.9	5.02
Mean	1450.37	88.41	25.38	5.08
Std.Dev	26.95	0.98	0.47	0.06
COV %	1.86%	1.11%	1.86%	1.11%
180W A	1669.50	66.34	29.2	3.657
180W B	1563.62	62.09	27.4	3.408
180W C	1757.24	69.88	30.8	3.855
Mean	1663.45	66.10	29.11	3.64
Std.Dev	96.95	3.90	1.70	0.22
COV %	5.83%	5.90%	5.83%	6.16%
140NW A	1571.39	93.73	27.5	5.38
140NW B	1541.82	92.88	27.0	5.33
140NW C	1543.98	93.25	27.0	5.35
Mean	1552.40	93.29	27.17	5.36
Std.Dev	16.49	0.42	0.29	0.02
COV %	1.06%	0.46%	1.06%	0.46%
EPS A	132.40	6.53	2.3	0.38
EPS B	134.92	6.64	2.4	0.38

Continued				
EPS C	164.63	8.10	2.9	0.47
Mean	143.98	7.09	2.52	0.41
Std.Dev	17.92	0.87	0.31	0.05
COV %	12.45%	12.34%	12.45%	12.34%

Table A.4. Water Retention Results

Specimen	Nominal Density	% Water Absorbed by Weight	% Water Absorbed by Volume	Average % Weight	Average % Volume	Stdev % Weight	Stdev % Volume
1	110W	23.3%	2.6%				
2	110W	23.1%	2.5%	22.8%	2.5%	0.7%	0.1%
3	110W	21.9%	2.4%				
1	140W	57.5%	8.6%				
2	140W	55.2%	8.2%	51.9%	7.7%	7.8%	1.2%
3	140W	43.0%	6.4%				
1	140NW	99.6%	14.7%				
2	140NW	102.1%	15.2%	110.0%	16.4%	15.9%	2.5%
3	140NW	128.3%	19.3%				
1	180W	14.6%	3.0%				
2	180W	14.3%	3.0%	13.9%	2.9%	1.0%	0.2%
3	180W	12.7%	2.7%				
1	EPS	54.3%	1.7%				
2	EPS	31.0%	0.9%	36.7%	1.1%	15.5%	0.5%
3	EPS	24.9%	0.7%				

Table A.5. Thermal Conductivity Results of Various WFI Products

Material	Replicate	Density (kg/m³)	Thermal Conductivity (W/(m*K))	Thermal Resistance ((m²*K)/W)	R-value(°F·ft²·h/BTU)	R-value/inch
110W	1	110.7	0.038	1.00	5.68	3.79
	2	109.8	0.038	1.01	5.72	3.82
	3	112.2	0.038	1.00	5.66	3.77
	4	111.9	0.038	1.00	5.69	3.79
Summary Statistics	Mean	111.15	0.038	1.00	5.69	3.79
	Stdev	1.11	0.000	0.00	0.03	0.02
	COV %	1.00%	0.48%	0.47%	0.47%	0.47%
140W	1	148.5	0.047	1.27	7.22	3.04
	2	147.9	0.047	1.28	7.29	3.07
	3	148.9	0.047	1.28	7.26	3.06
	4	147.6	0.047	1.29	7.34	3.09
Summary Statistics	Mean	148.23	0.047	1.28	7.28	3.07
	Stdev	0.59	0.000	0.01	0.05	0.02
	COV %	0.39%	0.70%	0.70%	0.70%	0.70%
180W	1	214	0.048	0.79	4.49	2.99
	2	213.8	0.048	0.79	4.47	2.98
	3	215.5	0.048	0.79	4.49	2.99
	4	214.9	0.048	0.79	4.47	2.98
Summary Statistics	Mean	214.55	0.048	0.79	4.48	2.99
	Stdev	0.79	0.000	0.00	0.01	0.01
	COV %	0.37%	0.28%	0.29%	0.29%	0.29%

Table A.6. Thermal Conductivity of Pilot-Scale Materials

Sample	Mean Temp. °C	Delta Temp. K	Heat Flux W/m²	Thermal Conductivity W/(m·K)	Thermal Resistance (m²·K)/W	Temp. Gradient K/m	R-value (°F·ft²·h /BTU)	R-value/ inch
EPS A.1	11.0	22.0	7.45	0.0337	2.95	220.85	16.76	4.27
	20.0	22.0	7.61	0.0345	2.89	220.83	16.41	4.18
	30.0	22.0	7.78	0.0352	2.93	220.86	16.63	4.24
	40.0	22.0	8.00	0.0362	2.75	220.88	15.62	3.98
	50.0	22.0	8.20	0.0371	2.68	220.83	15.23	3.88
	60.0	22.0	8.37	0.0379	2.63	220.87	14.92	3.80
	Mean		7.9	0.0400	2.81	220.85	15.93	4.06
	STDV		0.35	0.0016	0.14	0.02	0.78	0.199
	COV %		4.47	4.00	4.88	0.01	4.89	4.89
	Min		7.45	0.0337	2.63	220.83	14.92	3.80
	Max		8.37	0.0379	2.95	220.88	16.76	4.27
EPS A.2	11.0	22.0	7.45	0.0337	2.96	220.89	16.78	4.28
	20.0	22.0	7.61	0.0345	2.89	220.91	16.41	4.19
	30.0	22.0	7.78	0.0352	2.83	221.02	16.07	4.10
	40.0	22.0	7.99	0.0362	2.75	220.91	15.63	3.99
	50.0	22.0	8.20	0.0371	2.68	220.89	15.24	3.89
	60.0	22.0	8.38	0.0379	2.63	220.96	14.91	3.80
	Mean		7.90	0.0400	2.79	220.93	15.84	4.04
	STDV		0.36	0.0016	0.13	0.051	0.711	0.181
	COV %		4.50	4.00	4.49	0.02	4.49	4.49
	Min		7.45	0.0337	2.63	220.89	14.91	3.80
	Max		8.38	0.0379	2.96	221.02	16.78	4.28
EPS B.1	11.0	22.0	7.49	0.0339	2.94	220.68	16.69	4.25
	20.0	22.0	7.64	0.0346	2.88	220.65	16.35	4.16

Continued								
EPS B.1	30.0	22.0	7.80	0.0353	2.82	220.69	16.03	4.08
	40.0	22.0	8.00	0.0363	2.75	220.48	15.61	3.97
	50.0	22.0	8.22	0.0373	2.68	220.59	15.20	3.87
	60.0	22.0	8.39	0.0380	2.62	220.67	14.89	3.79
	Mean		7.92	0.0400	2.78	220.63	15.79	4.02
	STDV		0.35	0.0016	0.12	0.08	0.69	0.176
	COV %		4.38	4.00	4.37	0.04	4.37	4.37
	Min		7.49	0.0339	2.62	220.48	14.89	3.79
	Max		8.39	0.0380	2.94	220.69	16.69	4.25
	11.0	22.0	7.47	0.0339	2.95	220.64	16.73	4.26
	20.0	22.0	7.64	0.0346	2.88	220.58	16.34	4.16
	30.0	22.0	7.78	0.0353	2.83	220.56	16.04	4.09
	40.0	22.0	8.02	0.0364	2.74	220.65	15.57	3.97
	50.0	22.0	8.23	0.0373	2.67	220.54	15.18	3.87
EPS B.2	60.0	22.0	8.40	0.0381	2.62	220.63	14.87	3.79
	Mean		7.92	0.0400	2.78	220.6	15.79	4.02
	STDV		0.36	0.0016	0.13	0.05	0.710	0.181
	COV %		4.51	4.00	4.50	0.02	4.50	4.50
	Min		7.47	0.0339	2.62	220.54	14.87	3.79
	Max		8.40	0.0381	2.95	220.65	16.73	4.26
	11.0	22.0	7.48	0.0340	2.94	220.44	16.69	4.25
	20.0	22.0	7.65	0.0347	2.88	220.43	16.33	4.16
	30.0	22.0	7.82	0.0355	2.81	220.5	15.98	4.07
	40.0	22.0	8.04	0.0365	2.74	220.45	15.53	3.95
EPS C.1	50.0	22.0	8.24	0.0374	2.67	220.38	15.15	3.86
	60.0	22.0	8.41	0.0382	2.62	220.47	14.85	3.78
	Mean		7.94	0.0400	2.77	220.45	15.76	4.01
	STDV		0.36	0.0016	0.12	0.04	0.71	0.180

Continued

	COV %		4.00	4.00	4.00	0.00	4.48	4.48
	Min		7.48	0.0340	2.62	220.38	14.85	3.78
	Max		8.41	0.0382	2.94	220.5	16.69	4.25
	11.0	22.0	7.46	0.0339	2.95	220.41	16.74	4.26
	20.0	22.0	7.64	0.0347	2.88	220.46	16.35	4.16
	30.0	22.0	7.80	0.0354	2.82	220.44	16.01	4.08
	40.0	22.0	8.04	0.0365	2.74	220.44	15.54	3.95
	50.0	22.0	8.25	0.0374	2.67	220.39	15.14	3.85
EPS C.2	60.0	22.0	8.43	0.0382	2.61	220.48	14.82	3.77
	Mean		7.94	0.0400	2.78	220.44	15.77	4.01
	STDV		0.37	0.0017	0.13	0.03	0.73	0.186
	COV %		5.00	5.00	5.00	0.00	4.64	4.64
	Min		7.46	0.0339	2.61	220.39	14.82	3.77
	Max		8.43	0.0382	2.95	220.48	16.74	4.26
	11.0	22.0	9.54	0.0455	2.31	209.58	13.10	3.17
	20.0	22.0	10.38	0.0496	2.12	209.57	12.03	2.91
	30.0	22.0	11.45	0.0546	1.92	209.57	10.91	2.64
	40.0	22.0	9.92	0.0474	2.22	209.54	12.59	3.05
	50.0	22.0	9.93	0.0474	2.21	209.49	12.58	3.04
WFI A.1	60.0	22.0	9.71	0.0464	2.27	209.47	12.86	3.11
	Mean		10.15	0.0500	2.17	209.54	12.35	2.99
	STDV		0.69	0.0033	0.14	0.046	0.787	0.190
	COV %		7.00	7.00	6.00	0.00	6.37	6.37
	Min		9.54	0.0455	1.92	209.47	10.91	2.64
	Max		11.45	0.0546	2.31	209.58	13.10	3.17
	11.0	22.0	10.02	0.0479	2.19	209.45	12.46	3.01
WFI A.2	20.0	22.0	10.52	0.0502	2.09	209.53	11.87	2.87
	30.0	22.0	11.25	0.0537	1.96	209.5	11.10	2.69

Continued								
	40.0	22.0	11.88	0.0567	1.85	209.53	10.52	2.54
	50.0	22.0	9.15	0.0437	2.41	209.55	13.66	3.30
	60.0	22.0	8.58	0.0410	2.56	209.39	14.55	3.52
	Mean		10.23	0.0500	2.18	209.49	12.36	2.99
	STDV		1.25	0.0059	0.27	0.0608	1.53	0.37
	COV %		12.00	12.00	12.00	0.00	12.39	12.39
	Min		8.58	0.04	1.85	209.39	10.52	2.54
	Max		11.88	0.06	2.56	209.55	14.55	3.52
	11.0	22.0	9.94	0.0474	2.21	209.54	12.57	3.04
	20.0	22.0	10.66	0.0509	2.06	209.45	11.71	2.83
	30.0	22.0	10.03	0.0479	2.19	209.48	12.45	3.01
	40.0	22.0	9.58	0.0457	2.30	209.52	13.04	3.15
	50.0	22.0	9.57	0.0457	2.30	209.53	13.06	3.16
WFI B.1	60.0	22.0	9.48	0.0452	2.32	209.51	13.18	3.19
	Mean		9.88	0.0500	2.23	209.51	12.67	3.06
	STDV		0.44	0.0021	0.10	0.03	0.55	0.133
	COV %		4.00	5.00	4.00	0.00	4.35	4.35
	Min		9.48	0.0452	2.06	209.45	11.71	2.83
	Max		10.66	0.0509	2.32	209.54	13.18	3.19
	11.0	22.0	7.47	0.0339	2.95	220.64	16.73	4.05
	20.0	22.0	7.64	0.0346	2.88	220.58	16.34	3.95
	30.0	22.0	7.78	0.0353	2.83	220.56	16.04	3.88
	40.0	22.0	8.02	0.0364	2.74	220.65	15.57	3.77
WFI B.2	50.0	22.0	8.23	0.0373	2.67	220.54	15.18	3.67
	60.0	22.0	8.40	0.0381	2.62	220.63	14.87	3.60
	Mean		7.92	0.0400	2.78	220.60	15.79	3.82
	STDV		0.36	0.0016	0.13	0.05	0.71	0.172
	COV %		5.00	5.00	4.00	0.00	4.50	4.50

Continued								
	Min		7.47	0.0339	2.62	220.54	14.87	3.60
	Max		8.40	0.0381	2.95	220.65	16.73	4.05
WFI C.1	11.0	22.0	9.97	0.0476	2.21	209.53	12.53	3.03
	20.0	22.0	10.82	0.0516	2.03	209.5	11.55	2.79
	30.0	22.0	11.69	0.0558	1.88	209.54	10.69	2.58
	40.0	22.0	9.83	0.0469	2.24	209.55	12.72	3.08
	50.0	22.0	10.03	0.0479	2.19	209.56	12.46	3.01
	60.0	22.0	9.47	0.0452	2.33	209.62	13.20	3.19
	Mean		10.3	0.0500	2.15	209.55	12.19	2.95
	STDV		0.81	0.0039	0.16	0.04	0.91	0.221
	COV %		8.00	8.00	7.00	0.00	7.49	7.49
	Min		9.47	0.0452	1.88	209.50	10.69	2.58
	Max		11.69	0.0558	2.33	209.62	13.20	3.19
WFI C.2	11.0	22.0	10.05	0.0479	2.19	209.51	12.44	3.01
	20.0	22.0	10.49	0.0501	2.10	209.51	11.91	2.88
	30.0	22.0	11.31	0.0539	1.95	209.59	11.05	2.67
	40.0	22.0	12.08	0.0577	1.82	209.47	10.33	2.50
	50.0	22.0	9.15	0.0437	2.40	209.56	13.66	3.30
	60.0	22.0	8.53	0.0407	2.58	209.46	14.64	3.54
	Mean		10.27	0.0500	2.17	209.52	12.34	2.98
	STDV		1.32	0.0063	0.28	0.05	1.61	0.389
	COV %		13.00	13.00	13.00	0.00	13.02	13.02
	Min		8.53	0.0407	1.82	209.46	10.33	2.50
	Max		12.08	0.0577	2.58	209.59	14.64	3.54

Appendix B. Statistical Analysis of Testing Results

Table B.1. Tensile Panel Replicate Comparative Statistics

	EPI					
	WFI to SPF		WFI to OSB		WFI to WFI	
	EL A	EL B	EL A	EL B	EL A	EL B
	11.9	15.6	11.7	12.3	12.8	13.2
	16.2	14.8	12.5	12.5	13.6	13.4
	15.9	13.0	12.6	11.7	12.5	13.5
	12.8	14.9	13.0	11.2	11.0	11.1
Min	11.9	13.0	11.7	11.2	11.0	11.1
Max	16.2	15.6	13.0	12.5	13.6	13.5
Avg	**14.2**	**14.6**	**12.5**	**11.9**	**12.5**	**12.8**
Std.Dev	2.2	1.1	0.5	0.6	1.1	1.2
COV (%)	15.4	7.7	4.4	4.9	8.7	9.1
F-test	0.307		0.908		0.907	
T-test	0.780		0.234		0.694	

Continued	**PUR-R**					
	WFI to SPF		WFI to OSB		WFI to WFI	
	PUR-R A	PUR-R B	PUR-R A	PUR-R B	PUR-R A	PUR-R B
	11.9	14.1	11.7		13.0	11.5
	11.7	13.5	13.2	13.5	9.4	11.7
	11.9	14.6	13.8	14.0	10.0	8.5
	13.3	15.3	13.5	14.9	13.8	11.1
Min	11.7	13.5	11.7	13.5	9.4	8.5
Max	13.3	15.3	13.8	14.9	13.8	11.7
Avg	**12.2**	**14.4**	**13.0**	**14.2**	**11.5**	**10.7**
Std.Dev	0.7	0.8	0.9	0.7	2.2	1.5
COV (%)	5.8	5.3	7.1	5.2	19.0	14.1
F-test	0.923		0.824		0.556	
T-test	**0.006**		0.144		0.547	

Continued	PUR-S					
	WFI to SPF		WFI to OSB		WFI to WFI	
	PUR-S A	PUR-S B	PUR-S A	PUR-S B	PUR-S A	PUR-S B
	14.1	12.6	14.8	14.0	14.3	15.2
	11.2	15.0	15.4	16.0	15.3	15.7
	13.7	14.4	14.0	17.2	9.1	15.9
	13.9	14.5	14.8	14.6	14.1	12.5
Min	11.2	12.6	14.0	14.0	9.1	12.5
Max	14.1	15.0	15.4	17.2	15.3	15.9
Avg	**13.2**	**14.2**	**14.8**	**15.4**	**13.2**	**14.8**
Std.Dev	1.3	1.0	0.6	1.4	2.8	1.6
COV (%)	10.1	7.4	3.8	9.1	21.1	10.8
F-test	0.698		0.169		0.390	
T-test	0.306		0.403		0.352	

*Absent PUR-R value was removed as an extreme outlier that shifted the results of the statistical test

Table B.2. Two-way ANOVA of Tensile Strength Variables

Overall ANOVA

	DF	Sum of Squares	Mean Square	F Value	P Value
Adhesive	2	33.561	16.780	8.361	6.096E-4
Lamina	2	19.838	9.919	4.942	0.010
Interaction	4	37.904	9.476	4.721	0.002
Model	8	92.253	11.532	5.746	<0.0001
Error	62	124.429	2.007		
Corrected Total	70	216.683			
At the 0.05 level, the population means of Adhesive are significantly different. At the 0.05 level, the population means of Lamina are significantly different. At the 0.05 level, the interaction between Adhesive and Lamina is significant.					

Table B.3. Tensile Strength Means Comparison Groups

Adhesive's Grouping Letters Table

	Mean	Groups	
PUR-S	14.266	A	
EPI	13.069		B
PUR-R	12.603		B
Means that do not share a letter are significantly different.			

Lamina's Grouping Letters Table

	Mean	Groups	
WFI to SPF	13.788	A	
WFI to OSB	13.602	A	
WFI to WFI	12.590		B

Means that do not share a letter are significantly different.

Interactions 's Grouping Letters Table

Adhesive	Lamina	Mean	Groups		
PUR-S	WFI to OSB	15.094	A		
EPI	WFI to SPF	14.383	A	B	
PUR-S	WFI to WFI	14.018	A	B	
PUR-S	WFI to SPF	13.686	A	B	
PUR-R	WFI to OSB	13.509	A	B	
PUR-R	WFI to SPF	13.296	A	B	C
EPI	WFI to WFI	12.634		B	C
EPI	WFI to OSB	12.191		B	C
PUR-R	WFI to WFI	11.117			C

Means that do not share a letter are significantly different.

Table B.4. Two-way ANOVA of Shear Strength Variables

Overall ANOVA

	DF	Sum of Squares	Mean Square	F Value	P Value
Adhesive	2	610.193	305.096	3.519	0.035
Lamina	2	160.285	80.142	0.924	0.402
Interaction	4	587.351	146.837	1.694	0.162
Model	8	1378.907	172.363	1.988	0.062
Error	62	5373.926	86.676		
Corrected Total	70	6752.833			

At the 0.05 level, the population means of Adhesive are significantly different.
At the 0.05 level, the population means of Lamina are not significantly different.
At the 0.05 level, the interaction between Adhesive and Lamina is not significant

Table B.5. Shear Strength Means Comparison Groups

Adhesive's Grouping Letters Table

	Mean	Groups	
PUR-S	75.932	A	
PUR-R	69.874	A	B
EPI	69.412		B

Means that do not share a letter are significantly different.

Lamina's Grouping Letters Table

	Mean	Groups
WFI to WFI	73.586	A
WFI to SPF	71.775	A
WFI to OSB	69.937	A

Means that do not share a letter are significantly different.

Interactions 's Grouping Letters Table

Adhesive	Lamina	Mean	Groups
PUR-S	WFI to WFI	80.105	A
PUR-R	WFI to SPF	76.034	A
PUR-S	WFI to OSB	75.305	A
PUR-S	WFI to SPF	72.386	A
EPI	WFI to WFI	71.922	A
EPI	WFI to OSB	68.877	A
PUR-R	WFI to WFI	68.730	A
EPI	WFI to SPF	67.438	A
PUR-R	WFI to OSB	65.629	A

Means that do not share a letter are significantly different.

Table B.6. Statistical Analysis of Permeance and Permeability Results

Overall ANOVA

	DF	Sum of Squares	Mean Square	F Value	Prob>F
Model	4	16313.504	4078.376	1073.556	<0.0001
Error	10	37.989	3.798		
Total	14	16351.493			

Null Hypothesis: The means of all levels are equal. Alternative Hypothesis: The means of one or more levels are different. At the 0.05 level, the population means are significantly different.

Tukey Test

	Mean	Groups			
110-W	94.15661	A			
140-NW	93.2857	A	B		
140-W	88.41221		B		
180-W	66.10339			C	
EPS	7.08689				D

Means that do not share a letter are significantly different.

Appendix C. Moisture Content Verification

Table C. 1: Oven Dry Moisture Content Compared to Moisture Pin Measurements

Condition 1						
Sample	Wet (g)	Dry (g)	MC% Dry	Measured MC%	Adjustment Factor Dry	Difference Dry
A2	127.39	118.00	7.96%	6.95%	12.66%	1.01%
B2	131.70	121.10	8.75%	7.20%	17.74%	1.55%
C2	129.52	118.90	8.93%	7.15%	19.95%	1.78%
Condition 2						
Sample	Wet (g)	Dry (g)	MC% Dry	Measured MC%	Adjustment Factor Dry	Difference Dry
A1	137.01	119.25	14.89%	12.90%	13.38%	1.99%
B1	143.16	124.78	14.73%	13.50%	8.35%	1.23%
C1	141.07	123.95	13.81%	12.50%	9.50%	1.31%
Condition 3						
Sample	Wet (g)	Dry (g)	MC% Dry	Measured MC%	Adjustment Factor Dry	Difference Dry
A3	150.60	125.18	20.31%	19.50%	3.97%	0.81%
B3	157.02	128.59	22.11%	20.65%	6.60%	1.46%
C3	151.15	123.80	22.09%	20.10%	9.02%	1.99%
				Mean	**11.24%**	**1.46%**
				STDV	**5.19%**	**0.42%**
				COV %	**46.16%**	**28.52%**

BIOGRAPHY OF THE AUTHOR

Jacob Snow was born in Plainfield, Connecticut on October 23, 1999. He was raised in Plainfield and graduated from Plainfield Highschool in 2017. He attended the University of Maine and graduated with a Bachelor's degree in Forest Operations, Bioproducts, and Bioenergy, with a minor in Business Management in 2021. He remained at UMaine and entered the Bioproducts Engineering graduate program in the summer of 2021 immediately after completing his B.S. After completing his coursework, Jacob joined the Advanced Structures and Composites Center as a Wood Technologist to continue his career researching forest products. Jacob is a candidate for the Master of Science in Forest Resources from the University of Maine in August 2024.